Pun, B.K. et al. 2005. *Atmospheric Transformations*. Chapter 12 of *AIR QUALITY MODELING – Theories, Methodologies, Computational Techniques, and Available Databases and Software. Vol. II – Advanced Topics* (P. Zannetti, Editor). Published by The EnviroComp Institute (http://www.envirocomp.org/) and the Air & Waste Management Association (http://www.awma.org/).

Chapter 12

Atmospheric Transformations

Betty K. Pun [(1)], Christian Seigneur [(2)] and Hope Michelsen [(3)]

[(1)] *Atmospheric and Environmental Research, Inc., San Ramon, CA (USA)*
pun@aer.com
[(2)] *Atmospheric and Environmental Research, Inc., San Ramon, CA (USA)*
seigneur@aer.com
[(3)] *Sandia National Laboratories, Livermore, CA (USA)*
hamiche@ca.sandia.gov

Abstract: A typical air quality model tracks the transport and transformation of chemicals in the atmosphere. Transport refers to physical movement (dispersion, emissions, and deposition) of pollutants. Atmospheric transformations encompass both physical and chemical changes of chemicals in the atmosphere. In this chapter, we provide a review of the fundamentals of gas phase chemical reactions, phase transitions, aqueous phase reactions, and an overview of the key processes involved in the formation of ozone, particulate matter, hazardous air pollutants, and halogen chemistry. Modeling air quality entails the mathematical representation of the atmospheric transformations and the numerical solution of the algebraic equations and ordinary differential equations, which are developed in this chapter. The modeling of chemical transformations is discussed, starting with plume models and the gas-phase chemistry at different stages of the plume. We then describe several Eulerian models and their atmospheric mechanisms, including the Carbon Bond Mechanism (CBM)-IV, the Statewide Air Pollution Research Center mechanisms, the Regional Acid Deposition Model mechanism version 2, etc. The modeling of particulate matter and droplets requires a mathematical description of the aqueous-phase and heterogeneous chemistry. Modules that describe the gas/particle partitioning of inorganic species and organic species are discussed. The distribution of the semi-volatile products of gas-phase, aqueous, and heterogeneous reactions onto particles depends on the representation of the particle size distribution. In one-atmosphere approach, a single model would suffice if it included a comprehensive chemical mechanism containing all gas-phase, heterogeneous, and aqueous-phase reactions for all air pollutants of concern and a phase transition module describing all relevant dynamic processes for different types of particles. In practice, chemical mechanisms have been developed to describe the chemical transformation processes for different air pollutants. Therefore, in addition to models describing ozone and particulate matter (PM), specific models exist for hazardous air pollutants and other models describe the stratosphere. To complete the overview of available models for chemical transformations, plume-in-grid type models that combine plume chemistry with urban/regional chemistry are discussed.

Key Words: secondary air pollutants, urban ozone, particulate matter, stratospheric ozone, hazardous air pollutants, thermodynamics, atmospheric chemistry, radicals, heterogeneous and aqueous reactions, chemical mechanisms, kinetics, chemical transport models, plume-in-grid.

1 Introduction

The atmosphere can be viewed as a reactor of sorts, where anthropogenic and biogenic emissions undergo long- and short-range transport processes, chemical reactions, and phase transitions to produce the pollution problems that affect human health and ecological welfare. The role of atmospheric chemistry is particularly important in the following air pollution issues:

1. Tropospheric ozone (O_3) and photochemical smog
2. Fine particulate matter (PM), which also causes regional haze and visibility degradation
3. Global climate change
4. Acid deposition
5. Hazardous air pollutants
6. Stratospheric O_3 depletion

These problems range in geographical scales. Tropospheric O_3 and photochemical smog may be of urban to regional scale, and sometimes involve long range transport, e.g., up the East Coast of the United States or intercontinental transport from Asia to America (Berntsen et al., 1999; Jacob et al., 1999; Wilkening et al., 2000) or from America to Europe (Hogue, 2001). Fine PM[1] of aerodynamic diameter less than 2.5 μm ($PM_{2.5}$) is an urban pollutant implicated in increased incidences of cardiovascular and pulmonary illness (Health Effects Institute, 2001). On a regional scale, the same small particles contribute to haze and visibility reduction in pristine areas. Acid deposition is typically a regional problem involving acidic gases and PM. PM may also have a substantial influence in the Earth's climate via its effect on the global radiation budget and as cloud condensation nuclei. Toxic air pollutants, including transition metals and persistent organic pollutants, may have local, urban, regional, and global impacts. Halogen-containing compounds are the culprits for stratospheric ozone depletion, which is a global problem.

This chapter provides an overview of the atmospheric transformation processes that are relevant for the air pollution problems at hand. Sections 2 to 5 present the scientific fundamentals. Section 2 introduces gas-phase chemical reactions that are responsible for the formation of O_3 and other pollutants that constitute photochemical smog. In Section 3, we introduce heterogeneous processes, which involve either phase transition or chemical reactions in a liquid phase. Sections 4 and 5 are devoted to the discussions of air toxics and halogen chemistry, respectively. For more details, the readers can refer to any of a number of

[1] The term "fine PM" refers to $PM_{2.5}$ in the United States but to PM_{10} in Europe. We adopt the United States convention in this chapter.

atmospheric chemistry textbooks, including Finlayson-Pitts and Pitts (2000), Seinfeld and Pandis (1998), Wayne (1991), and Warneck (1988). Mathematical representation and current models for urban-regional air pollution are discussed in Sections 6 to 9. Section 6 focuses on the modeling of gas-phase processes. The mathematical techniques for heterogeneous and aqueous processes are discussed in Section 6. In Section 8 we will discuss plume models. We finish Section 8 with plume-in-grid models, which provide more detailed treatment of atmospheric dispersion of large point sources than Eulerian models, and include relevant chemistry for plumes with higher concentrations than the conditions treated in Eulerian models. In Section 9, we start with the Eulerian models that describe the atmospheric chemistry and transport processes. Additional details of air quality models can be found in Jacobson (1999) and Seinfeld and Pandis (1998) and a number of reviews that are mentioned in the text. Available modeling resources on the World Wide Web include the Community Modeling and Analysis System website (www.cmascenter.org).

2 Gas-Phase Transformations

Atmospheric reactions frequently involve free radicals. Free radicals are reactive species with unpaired electrons in their outer shells. A typical oxidant in the lower atmosphere is the hydroxyl radical (OH). In a hydroxyl radical, the oxygen atom has a total of 7 electrons on its outermost shell (Figure 1), which needs 8 to fill. Therefore, the OH radical has a tendency to snatch hydrogen atoms from other molecules to form a stable water molecule (all outer shells filled).

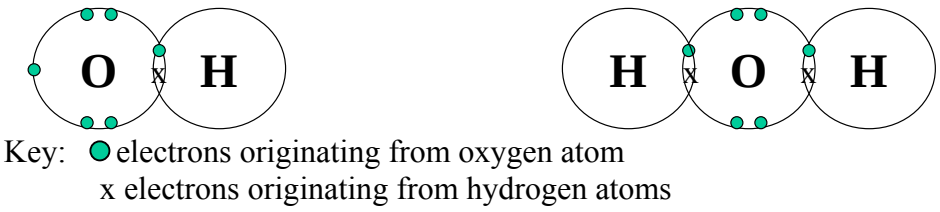

Figure 1. Electronic structures of hydroxyl radical and water molecule.

The molecule that lost a hydrogen atom becomes a free radical. Hence, free radical reactions typically generate free radicals in a chain of reactions. These reactions are terminated when two free radicals combine to form a stable molecule.

2.1 Chemistry of Nitrogen and Oxygen Species

So how do free radicals come about? Typically the formation of free radicals involves breaking a bond (a pair of electrons shared by two atoms) in a stable molecule to form two radicals with unpaired electrons. Solar radiation usually provides the burst of energy required for breaking up a bond. Many stable

molecules absorb photons with specific wavelengths or energy content. If the absorbed energy is large enough (larger than the strength of the bond holding the molecule together), the molecule may break apart and form radicals. This type of reaction is called photolysis in atmospheric chemistry. An example is the photolysis of nitrogen dioxide (NO_2)

$$NO_2 + h\nu \rightarrow NO + O \quad (1)$$

In the above reaction, hν denotes a photon that is absorbed by NO_2. NO_2 absorbs over the entire range of UV and visible radiation in the solar spectrum (wavelengths of 300-700 nm). The dissociation of NO_2 forms a nitric oxide (NO) and an oxygen atom. NO is a radical that is stabilized through a process called resonance, meaning that the unpaired electron is delocalized and can be associated with either the N atom or the O atom. The O atom typically reacts with an oxygen molecule (O_2) in the lower troposphere in a combination reaction:

$$O + O_2 + M \rightarrow O_3 + M \quad (2)$$

In this reaction, M denotes a third body (typically nitrogen (N_2) or O_2 gas) that serves to remove the excess energy released in the combination of O with O_2. The resulting molecule is O_3, which is the key component of photochemical smog. O_3 is chemically reactive, although it is not considered a free radical. The reaction between O_3 and NO is fast

$$O_3 + NO \rightarrow NO_2 + O_2 \quad (3)$$

At night, when the photolytic Reaction 1 stops due to the lack of sunlight, Reaction 3 controls the concentrations of O_3, NO, and NO_2. As Reaction 3 goes to completion, either O_3 or NO will be depleted, and the more abundant compound will coexist with NO_2. During the day, Reactions 1, 2, and 3 would be in a photostationary state in an atmosphere that contains only nitrogen and oxygen species. Under photostationary state conditions, the relative concentrations of O_2, O_3, NO, and NO_2 would remain constant as the cycle of reactions churns around. (We will discuss the concept of photostationary state some more when we talk about reaction kinetics in Section 6.) However, the stationary state of Reactions 1, 2, and 3 is modified by the presence of hydrogen and carbonaceous species.

2.2 Carbon and Hydrogen Perturbation of N-O Chemistry

The photostationary state established by Reactions 1, 2, and 3 is perturbed by the presence of OH and carbonaceous species (e.g., CO, methane) even in remote locations. OH originates from the photolysis of O_3

$$O_3 + h\nu \rightarrow O(^1D) + O_2 \quad (4)$$

$O(^1D)$ is an oxygen atom in an excited electronic state. It has sufficient energy to break up a water molecule. Two OH radicals are formed in this reaction.

$$O(^1D) + H_2O \rightarrow OH + OH \quad (5)$$

OH is considered the main oxidant in the lower atmosphere. For example, it reacts with carbon monoxide and methane; both are quite ubiquitous in the atmosphere.

$$OH + CO \rightarrow CO_2 + H \quad (6)$$

$$OH + CH_4 \rightarrow H_2O + CH_3 \quad (7)$$

Both H and CH_3, the simplest alkyl group, are very reactive radicals that combine with O_2 in the lower atmosphere to form the hydroperoxyl and methylperoxyl radicals:

$$H + O_2 \rightarrow HO_2 \quad (8)$$

$$CH_3 + O_2 \rightarrow CH_3O_2 \quad (9)$$

When NO is present in the atmosphere, the main reactions for the peroxyl radicals are

$$HO_2 + NO \rightarrow OH + NO_2 \quad (10)$$

$$CH_3O_2 + NO \rightarrow CH_3O + NO_2 \quad (11)$$

Therefore, the peroxyl radicals do the work for O_3 in Reaction 3. Since NO_2 photolyzes and eventually leads to the formation of O_3 (Reactions 1 and 2), its formation without consuming O_3 allows more O_3 to exist in an environment with a source of peroxyl radicals than in an oxygen-nitrogen atmosphere. In Reaction 10, OH is regenerated, and can initiate another cycle of reactions. In Reaction 11, the methoxyl radical product can continue the chain of reactions.

2.3 Complex Organics and Smog Formation

We continue with the reactions of the methoxyl radical, which is the simplest of all alkoxy radicals. The methoxyl radical reacts with O_2 and forms HO_2 and formaldehyde (HCHO).

$$CH_3O + O_2 \rightarrow HO_2 + HCHO \quad (12)$$

More complex alkoxy radicals can also decompose into alkyl radicals and carbonyl compounds (aldehydes and ketones), or undergo isomerization to generate an alkyl radical with a hydroxy functional group. For these reactions,

the readers may refer to detailed discussions found in Atkinson (1997). We are going to focus on the simpler reactions for illustrative purposes. Of the products of Reaction 12, the fate of HO_2 has been discussed. What happens to the HCHO?

HCHO is the simplest homologue of aldehydes (RCHO). Aldehydes and other carbonyls, i.e., compounds containing the double-bonded carbon-oxygen moiety (C=O) are products of the atmospheric oxidation of many aliphatic hydrocarbons, such as alkanes, alkenes, and alcohols.

Formaldehyde and other simple carbonyls may undergo photolysis. For example,

$$HCHO + h\nu \rightarrow CO + H_2 \quad (13)$$

$$HCHO + h\nu \rightarrow H + HCO \quad (14)$$

Reaction 13 produces stable products, while Reaction 14 leads to the formation of two new radicals. Reaction 14 is an example of an "initiation" reaction in the terminology of radical reactions. All aldehydes also react with OH, e.g.,

$$HCHO + OH \rightarrow H_2O + HCO \quad (15)$$

Like its unsubstituted counterpart, CH_3, HCO quickly reacts with O_2

$$HCO + O_2 \rightarrow HO_2 + CO \quad (16)$$

However, the larger members of the acyl radical family combine with O_2

$$CH_3CO + O_2 \rightarrow CH_3C(O)O_2 \quad (17)$$

Here, the (O) notation represents a carbonyl bond. This acyl peroxyl radical may undergo an analogous reaction to Reaction 11, or it may also react with NO_2 in a combination reaction

$$CH_3C(O)OO + NO_2 \rightarrow CH_3C(O)OONO_2 \quad (18a)$$

The product of this reaction is a peroxy acetyl nitrate, or PAN. The net effect of Reaction 18a is the removal of a radical, and this reaction can therefore be considered a "termination" reaction. However, this radical removal is not permanent, as PAN can dissociate back into the reactants

$$CH_3C(O)OO + NO_2 \leftarrow CH_3C(O)OONO_2 \quad (18b)$$

An example of a more permanent termination product is nitric acid (HNO_3)

$$OH + NO_2 \rightarrow HNO_3 \quad (19)$$

In environments where NO_x is not abundant, organic radicals may react with HO_2 in another termination reaction, e.g.,

$$CH_3C(O)OO + HO_2 \rightarrow CH_3C(O)OH + O_3 \quad (20a)$$

$$CH_3C(O)OO + HO_2 \rightarrow CH_3C(O)OOH + O_2 \quad (20b)$$

Without these termination reactions, alkyl radicals, such as that formed in Reaction 11, will continue generating carbonyls and more radicals. The cycle of reactions HO_2/OH and RO_2/RO converts NO to NO_2, which then photolyzes to produce O_3. These reaction cycles are depicted in Figure 2. Hence, the presence of organic compounds enhances the formation of O_3 via the reactions of organic radicals with NO_x.

We have used simple alkanes and aldehydes to illustrate the atmospheric radical chain reactions involving volatile organic compounds (VOC) that are responsible for the formation of smog. In addition to alkanes and aldehydes, other classes of VOC, such as alkenes and aromatic compounds, also participate in smog-producing reactions. Alkenes can be of anthropogenic and biogenic origins, and are typically quite reactive towards OH, O_3, and NO_3. Aromatic compounds react typically with OH; certain ones also react with NO_3. However, the current understanding of aromatic chemistry is incomplete, so that many of the secondary products remain unidentified. Nonetheless, both classes of compounds are of interest as precursors to secondary organic aerosols, as discussed in Section 2.4.

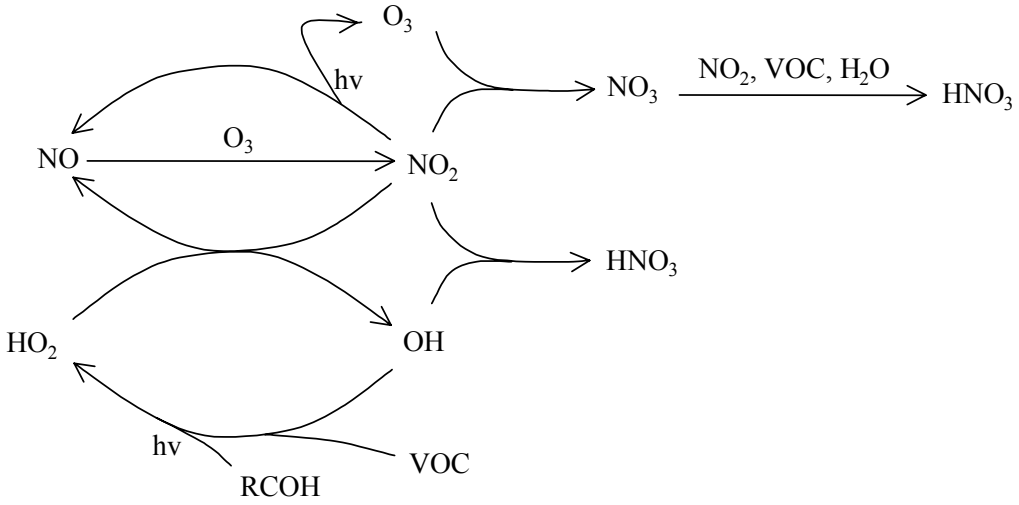

Figure 2. Major chemical cycles involved in the gas-phase production of secondary pollutants, O_3 and HNO_3 (Source: Pun et al., 2001; reprinted with permission of A&WMA).

2.4 Gas-Phase Formation of Condensable Compounds

Organic compounds with certain properties may partition out of the gas phase and into particles. Typically, the affinity for the gas phase is reflected in a compound's saturation vapor pressure - the higher the saturation vapor pressure, the more likely a compound will stay in the gas phase, and vice versa. The presence of functional groups decreases the saturation vapor pressure of a compound. Because functional groups also tend to be more polar than hydrocarbons, functional groups may also increase the water solubility of an organic compound. Solubility and vapor pressure are two parameters that govern the affinity of a compound towards aqueous or organic liquid (or in some cases, solid) phases that are likely to be present in atmospheric particles. Many organic compounds, especially those containing functional groups, have been identified in atmospheric particles. Table 1 lists some of these compounds.

Table 1. Organic compounds in atmospheric particles (source: Saxena and Hildemann, 1996; Schauer and Cass, 1999).

Saxena and Hildemann, 1996	Schauer and Cass, 1999
C10-C34 n-alkanes	Alkanes
C9-C30 n-alkanoic and n-alkenoic acids & their esters	n-alkanoic acids
C10-C35 n-alkanols	n-alkenoic acids
C9, C14 aldehydes	Dicarboxylic acids
Dehydroabietic and other diterpenoid acids and retene	Syringol and substituted syringols
Phthalic and other aromatic polycarboxylic acids & their esters	Aromatic acids
Polycyclic aromatic hydrocarbons (PAH)	PAH
Polycyclic aromatic ketones and quinones	Guaiacols and substituted guaiacols
Cholesterol and other steroids	Substituted phenols
1,2-dimethoxy-4-nitro-benzene and other aromatic N-containing compounds	Resin acids
Lignans	Sugars
Cellulose	

Some compounds listed in Table 1 are emitted directly, either as semi-volatile gases or as particles. In fact, many of the compounds listed in Table 1 are so unique to particular sources that they can be used as tracers to establish the presence or even the fractional contribution of particular sources to particles in an area. Compounds with functional groups can also be formed in the atmosphere. As we have seen in Section 2.3, gas-phase chemical reactions of volatile organic compounds can result in the formation of products that contain functional groups.

These products include aldehydes, ketones, carboxylic acids, alcohols, and nitrates.

Compounds with multiple functional groups are of interest because they can dissolve in aqueous particles that are quite ubiquitous in the lower troposphere. Pun et al. (2000) have investigated the formation of multifunctional compounds from volatile precursors. They concluded that many simple hydrocarbons may act as precursors to very complex organic products, especially via several generations of intermediates. Table 2 shows several classes of multifunctional compounds that may be present in the particulate phase and their possible precursors. These precursor-product relationships were determined based on known gas-phase reactions of which those described in the earlier sections of this chapter are a subset.

Table 2. Multi-functional compounds and likely precursors (source: Pun et al., 2000).

Compounds	Precursors	Intermediates
Dicarboxylic Acids	Diene	Unsat. Monocarboxylic Acid
	Diene	Unsat. Monocarboxylic Acid Unsat. Aldehyde
Dicarboxylic Acids	(ω)-Oxo-Monocarboxylic Acid	See ketoacid entries
α, β Dicarbonyls	Aromatic Compounds	
Dicarbonyls	(a) Cycloalkene / (b) Cycloalkane	
	(a) Alkane / (b) Alkene / (c) Alcohol	Ketone
	Diene	Unsaturated Carbonyl*
	(a) Alkane / (b) Alkene / (c) Unsaturated alcohol / (d) Polyol	Hydroxy Ketone
Ketoacids	Cycloalkene	
	Alkene	Carboxylic Acid
	(a) Alkane / (b) Alkene / (c) Alcohol	Carboxylic Acid, aldehyde
	Diene	Unsaturated Carboxylic Acid
	Diene	Unsaturated Carboxylic Acid, Unsaturated Aldehyde
	Hydroxyacid (see below for secondary formation)	
	Diene	Unsaturated Carbonyl
	Dicarbonyl (Ketoaldehyde) (see above for secondary formation)	
Polyols, e.g. Polyhydroxycarbonyls (Secondary poly-hydroxy compounds also contain carbonyl groups)	Alkane (branched)	
Polyhydroxycarbonyls	Alkene (especially α, β-dihydroxy product) (or) Unsaturated alcohol	

	Branched alcohol	
	Polyol	
Multifunctional compounds # Hydroxycarboxylic Acids	Hydroxy-Alkene	
	Diene	Hydroxy-oxo-alkene
	(a) Alkane / (b) Alkene / (c) Unsat. Alcohol / (d) Branched alcohol / (e) Diol	Hydroxyaldehyde see analogous polyhydroxycarbonyl entries
Hydroxycarboxylic Acids	Diene	Hydroxy-oxo-alkene
Hydroxy-oxo-carboxylic Acids	Diene	Unsat. Carboxylic Acid
	Diene	Unsat. Carboxylic Acid, Unsat. Aldehyde
	Alkene	Carboxylic Acid
Hydroxy-oxo-carboxylic Acids	(a) Alkane / (b) Alkene / (c) Alcohol	Carboxylic Acid, Aldehyde
Nitrophenols	Aromatic compounds	(Phenol)

* Unsaturated carbonyl compounds may be emitted from vegetation.
# Multifunctional compounds with acidic / basic and carbonyl groups

3 Heterogeneous and Aqueous Processes

Whereas gas-phase chemistry plays an important role in air pollution problems, the roles of heterogeneous and aqueous processes are also vital in the production of $PM_{2.5}$, regional haze/visibility degradation, and acid deposition. These processes include phase transition, a physical process, and heterogeneous and aqueous chemical reactions. In this section, we focus primarily on secondary pollutants, nitrate, sulfate, and secondary organic aerosol (SOA), but also note that some of the gas/particle conversion processes are also relevant for primary semi-volatile species.

3.1 Gas/Particle Conversion of Inorganic Species

Key inorganic species that convert between gas and particulate phases include sulfuric acid/sulfate, nitric acid/nitrate, hydrochloric acid/chloride, ammonia/ammonium, carbon dioxide/carbonate, and, most definitely, vapor/particulate water. Other non-volatile ions that affect the conversion of these species include sodium, calcium, magnesium, and potassium.

Sulfuric acid (H_2SO_4) and nitric acid (HNO_3) are formed in the atmosphere from emissions of sulfur dioxide (SO_2) and nitrogen oxides (NO_x). In the gas phase, sulfur trioxide (SO_3), which hydrolyzes to form H_2SO_4, is formed in a reaction of SO_2 with OH:

$$SO_2 + OH \rightarrow HOSO_2$$

$$HOSO_2 + O_2 \rightarrow SO_3 \qquad (21)$$

Nitric acid can be formed when NO_2 is oxidized in the atmosphere by OH or O_3:

$$NO_2 + OH \rightarrow HNO_3 \quad (22)$$

$$NO_2 + O_3 \rightarrow NO_3 + O_2 \quad (23)$$

$$NO_3 + NO_2 \rightarrow N_2O_5 \quad (24)$$

$$N_2O_5 + H_2O \rightarrow 2HNO_3 \quad (25)$$

Reaction 22 takes place during the day because the concentration of OH drops quickly after sunset. On the other hand, NO_3 tends to photolyze during the day, and the pathway involving NO_3 as an intermediate (24, 25) takes place primarily at night. In addition to the above reactions, HNO_3 is also formed when NO_3 radical abstract hydrogen atoms from hydrocarbons in reactions similar to those discussed in Section 2.2 for the OH radical. There are also two heterogeneous reactions that convert NO_3 or N_2O_5 to HNO_3. These reactions will be discussed in detail in Section 3.4.

Of the other species that participate in gas/particle conversion, chloride is typically emitted as sea salt particles (as sodium chloride), NH_3 is emitted in gaseous form, and carbonate is emitted in solid form as soil dust with potassium, calcium, and magnesium.

Atmospheric compounds sometimes exist in several states simultaneously. For example, under some conditions, molecular ammonia can exist in the gas phase and the aqueous phase. At the same time, it can be present as ammonium ion. Typically, a species will move from a medium with higher concentration to a medium with lower concentration. Here, concentration may be viewed as the driving force to move from one phase to the other. In the language of thermodynamics, fugacity or activity is used to define this driving force. Any system will progress towards a state of equilibrium between different phases, where the driving force to move from one phase to another is equilibrated between different phases. Some systems may take a long time to reach equilibrium while others reach it almost instantaneously.

The concentrations of the gas-phase and particulate-phase species involved in a thermodynamic equilibrium are typically governed by an equilibrium partition constant. We will explain later how to model equilibria mathematically. We simply note at this point that many species can be in equilibrium with one another simultaneously. For example, in the ammonium/nitrate/sulfate system, the equilibrium relationships that are satisfied are listed in Table 3. Further discussion of the gas/particle (gas/liquid) partitioning process is provided in the aqueous chemistry section (Section 3.3). We will explain the mathematical formulation in greater detail in Section 6. Some of these relationships are between the gas phase and the particle/droplet phase. Other equilibria are

between different aqueous molecules and ions, such as sulfate/bisulfate or aqueous ammonia/ammonium, or between solid species and ions. These equilibrium relationships are functions of temperature, pressure, and relative humidity. For example, higher temperatures favor the gaseous state over the solid or liquid states. Relative humidity governs the amount of water in aqueous particles or droplets, and hence affects aqueous-phase concentrations.

Table 3. Equilibrium relationships in the ammonium/nitrate/sulfate system (source: Nenes et al., 1998).

Reaction	Expression	Equilibrium constant at 298K	Units
$HSO_{4(aq)}^{-} \leftrightarrow H_{(aq)}^{+} + SO_{4(aq)}^{2-}$	$\frac{\left[H^{+}\right]\left[SO_4^{2-}\right]}{\left[HSO_4^{-}\right]}\frac{\gamma_{H^+}\gamma_{SO_4^{2-}}}{\gamma_{HSO_4^{-}}}$	0.01015	Mol kg^{-1}
$NH_{3(g)} \leftrightarrow NH_{3(aq)}$	$\frac{\left[NH_3\right]}{P_{NH_3}}\gamma_{NH_3}$	57.64	Mol kg^{-1} atm^{-1}
$NH_{3(aq)} + H_2O_{(aq)} \leftrightarrow NH_{4(aq)}^{+} + OH_{(aq)}^{-}$	$\frac{\left[NH_4^{+}\right]\left[OH^{-}\right]}{\left[NH_{3(aq)}\right]a_w}\frac{\gamma_{NH_4^+}\gamma_{OH^-}}{\gamma_{NH_3}}$	1.805 x 10^{-5}	Mol kg^{-1}
$HNO_{3(g)} \leftrightarrow H_{(aq)}^{+} + NO_{3(aq)}^{-}$	$\frac{\left[H^{+}\right]\left[NO_3^{-}\right]}{P_{HNO_3}}\gamma_{H^+}\gamma_{NO_3^{-}}$	2.511 x 10^{6}	Mol^2 kg^{-2} atm^{-1}
$H_2O_{(aq)} \leftrightarrow H_{(aq)}^{+} + OH_{(aq)}^{-}$	$\frac{\left[H^{+}\right]\left[OH^{-}\right]}{a_w}\gamma_{H^+}\gamma_{OH^-}$	1.01 x 10^{-14}	Mol^2 kg^{-2}
$(NH_4)_2SO_{4(s)} \leftrightarrow 2NH_{4(aq)}^{+} + SO_{4(aq)}^{2-}$	$\left[NH_4^{+}\right]^2\left[SO_4^{2-}\right]\gamma_{NH_4^+}^{2}\gamma_{SO_4^{2-}}$	1.817	Mol^3 kg^{-3}
$(NH_4)NO_{3(s)} \leftrightarrow NH_{3(g)} + HNO_{3(g)}$	$P_{NH_3}P_{HNO_3}$	5.746 x 10^{-17}	Atm^2
$(NH_4)HSO_{4(s)} \leftrightarrow NH_{4(aq)}^{+} + HSO_{4(aq)}^{-}$	$\left[NH_4^{+}\right]\left[HSO_4^{-}\right]\gamma_{NH_4^+}\gamma_{HSO_4^{-}}$	1.383	Mol^2 kg^{-2}
$(NH_4)_3H(SO_4)_{2(s)} \leftrightarrow 3NH_{4(aq)}^{+} + HSO_{4(aq)}^{-} + SO_{4(aq)}^{2-}$	$\left[NH_4^{+}\right]^3\left[HSO_4^{-}\right]\left[SO_4^{2-}\right]\times \gamma_{NH_4^+}^{3}\gamma_{HSO_4^{-}}\gamma_{SO_4^{2-}}$	29.72	Mol^5 kg^{-5}

3.2 Gas/Particle Conversion Process of Organic Species (Condensation)

The understanding of gas/particle partition of organic compounds is still in its infancy compared to that of the inorganic compounds. Organic aerosols consist of hundreds of compounds, including many that have not been identified. Some of these compounds may be primary, i.e., non-volatile compounds emitted as

particles or semi-volatile compounds that may be emitted as gases. Others may be secondary, i.e., condensable products formed from the oxidation of volatile compounds, as discussed in Section 2.4. Gas/particle partition has been studied for some individual compounds that have been identified in atmospheric organic particles. However, for complex systems, such as the formation of secondary organic aerosol (SOA) from the oxidation of VOC, the current understanding is based largely on empirical data, typically derived from environmental chambers.

Several theories have been presented in the literature for the equilibrium partition of organic compounds between gases and particles: dissolution, saturation, absorption, adsorption, etc. Soluble species like formic acid, acetic acid, and formaldehyde enter the particulate phase through dissolution into particles or into fog/cloud droplets. However, dissolution as a gas/particle conversion pathway has typically only been studied for systems with few components (Jacobson, 1999 and references therein). The formation of SOA when the gas-phase concentration reaches saturation is determined by the saturation vapor pressure at the given temperature. The saturation vapor pressure is the concentration in the gas phase that is in equilibrium with the pure liquid of the condensing species. The implicit assumption is that the particle contains a liquid phase of the pure liquid. A less stringent assumption, that the particle contains a liquid mixture, gives rise to several absorption theories. Because "like dissolves like", organic vapors are assumed to be absorbed into a liquid mixture of organic compounds in many absorption theories.

In addition to absorption, adsorption onto organic particles was shown to be a key mechanism through which semi-volatile organic compounds partition into the particle phase (Dachs and Eisenriech, 2000). A gas-phase compound adsorbs onto a particle's surface, which is different from absorptive partition, in which the gas-phase compounds enter the bulk phase of the particle.

3.3 Aqueous Chemistry

Clouds and fogs can play an important role in the chemistry of atmospheric species, as some reactions taking place in the aqueous phase are sufficiently fast in altering the chemical composition of the atmosphere significantly. Before aqueous reactions can occur, some reactants and products need to be transferred from the gas phase into the droplet phase and vice versa. This gas/particle transfer involves the dissolution of gas-phase species or the evaporation of aqueous species. In Section 2.1, we discussed the relevant gas/particle equilibria. Table 4 presents gas/liquid equilibria for selected atmospheric species active in aqueous chemistry. In addition to the partition between the gas and particle/droplet phase, ionization is also a common process that takes place in both particles and droplets. Table 5 summarizes the ionic dissociation equilibria of SO_2 (H_2SO_3), H_2SO_4, HNO_3, NH_3 (NH_4OH), CO_2 (H_2CO_3), and H_2O. In Section 6.2, we will discuss the mathematical formulations of the partition of

chemical species between the gas phase and the droplet phase, and address the ionic balance within the droplets and the calculation of pH.

In theory, aqueous chemical transformations can take place within aqueous particles. However, their liquid water content is not sufficient to lead to significant amounts of chemical conversion (Saxena and Seigneur, 1987; Meng and Seinfeld, 1994). Therefore, we focus here on the chemical transformations taking place in cloud and fog droplets. We will review the chemical transformations of sulfur, nitrogen, organic species, and oxygen species.

3.3.1 Sulfur Species

Cloud and fog droplets act as chemical reactors for the conversion of SO_2 to sulfate. The three major reactions are the oxidation of SO_2 by H_2O_2, O_3 and O_2. The latter reaction must be catalyzed by Fe^{3+} or Mn^{2+} to proceed at a significant rate. Other oxidants such as dichloride ions (Cl_2^-), organic peroxides, free radicals and NO_2 may also contribute to SO_2 oxidation under special conditions.

The H_2O_2 reaction involves several mechanistic steps. This reaction is relatively insensitive to the acidity, which is measured by the pH ($-\log_{10}[H^+]$) of a droplet, in the range of pH encountered in the fog and cloud droplets of the lower atmosphere. Therefore, H_2O_2 represents a key oxidant for SO_2 in a lot of tropospheric environments.

The reaction of SO_2 with O_3 is a strong function of pH. Since its rate decreases with decreasing pH, this reaction is self-limiting (the sulfate formed during the reaction leads to a lower pH). This reaction is most important at pH values above 4.

The reaction of SO_2 with O_2 must be catalyzed by trace metals (Fe^{3+} and Mn^{2+}) to proceed at a significant rate. The rates of the reactions differ for various pH ranges. In addition, the kinetics depend on the ionic strength of the solution and the presence of organic compounds. Moreover, there is synergism if both trace metals are present.

3.3.2 Nitrogen Species

Nitrate formation is also enhanced by the presence of cloud and fog droplets. The two major reactions are the hydrolysis of N_2O_5 to two molecules of HNO_3 and the conversion of the NO_3 radical to the NO_3^- ion. These reactions are very fast in solution and their kinetics can be assumed to be limited by the gas/droplet mass transfer step. For N_2O_5 and NO_3 gas-phase molecules that reach a droplet, the probabilities that they will be scavenged by a droplet are in the range of 0.01 to 1.0 for N_2O_5 and 10^{-4} to 10^{-2} for NO_3 (Jacob, 2000). Therefore, nitrate formation will proceed at a significant rate when N_2O_5 and NO_3 are present, i.e., primarily during nighttime.

Other reactions also lead to nitrate formation in the aqueous phase. For example, NO_2 undergoes a disproportionation reaction to form HNO_2 and HNO_3. However, NO_2 has a low solubility and this reaction is not a major pathway for nitrate formation.

3.3.3 Organic Species

Organic species that contain polar functional groups and have low to moderate molecular weights can dissolve in cloud and fog droplets. Such species include aldehydes, acids and organic nitrate species. Some of those species may interfere with sulfur chemistry (i.e., formation of hydromethanesulfonic acid or HMSA). Also, some organic chemical reactions may take place in solution. For example, Aumont et al. (2000) considered that VOC could be oxidized in droplets by OH radicals. Aldehydes could be converted to carboxylic acids, secondary alcohols to ketones and primary alcohols to carboxylic acids via aldehydes. Such oxidation reactions can lead to the formation of organic compounds that are more conducive to condensation than the original compounds, thereby leading to secondary organic aerosol formation.

3.3.4 Oxidant Species

Radicals such as OH and HO_2 can be scavenged by droplets. Jacob (2000) estimated that the probability for HO_2 scavenging was in the range of 0.1 to 1.0. In droplets, HO_2 radicals can combine to form H_2O_2. As discussed above, H_2O_2 is a major oxidant for sulfate formation.

The scavenging of radicals by droplets also has a profound effect on oxidant formation. As their gas-phase concentrations decrease due to scavenging by droplets, the photochemical formation of O_3 and OH will decrease. The effect of clouds on oxidant formation was first identified by Seigneur and Saxena (1985) and has been studied by several others since (e.g., Monod and Carlier, 1999; Jacob, 2000). In addition to the scavenging of radicals by droplets, the solubility of organic species, such as aldehydes, that are key precursors of radicals in the gas phase also affect O_3 chemistry.

Table 4. Gas/liquid equilibria of selected species (Jacobson, 1999; Seinfeld and Pandis, 1998).

Gas/liquid equilibrium	Henry's law coefficient at 25° C (M/atm)
SO_2 (g) ↔ SO_2 (aq)	1.22
HNO_3 (g) ↔ HNO_3 (aq)	2.10×10^{5}
H_2SO_4 (g) ↔ H_2SO_4 (aq)	∞
NH_3 (g) ↔ NH_3 (aq)	5.76×10^{1}
CO_2 (g) ↔ CO_2 (aq)	3.41×10^{-2}
O_3 (g) ↔ O_3 (aq)	1.13×10^{-2}
NO (g) ↔ NO (aq)	1.9×10^{-3}
NO_2 (g) ↔ NO_2 (aq)	1.00×10^{-2}
H_2O_2 (g) ↔ H_2O_2 (aq)	7.45×10^{4}

Table 5. Dissociation equilibria of selected species (Jacobson, 1999).

Equilibrium reactions	Equilibrium coefficient at 25° C (M)
H_2SO_3 (aq) $\leftrightarrow$ $HSO_3^- + H^+$	1.71×10^{-2}
HSO_3^- $\leftrightarrow$ $SO_3^{2-} + H^+$	5.99×10^{-8}
H_2SO_4 (aq) $\leftrightarrow$ $HSO_4^- + H^+$	1.00×10^{3}
HSO_4^- $\leftrightarrow$ $SO_4^{2-} + H^+$	1.02×10^{-2}
NH_4OH (aq) $\leftrightarrow$ $NH_4^+ + OH^+$	1.81×10^{-5}
H_2CO_3 (aq) $\leftrightarrow$ $HCO_3^- + H^+$	4.30×10^{-7}
HCO_3^- $\leftrightarrow$ $CO_3^{2-} + H^+$	4.68×10^{-11}
H_2O (l) $\leftrightarrow$ $H^+ + OH^-$	1.01×10^{-14}

3.4 Heterogeneous Chemistry

Heterogeneous chemistry refers to chemical reactions that involve two phases. These reactions may take place on the surface of particles, or in the bulk phase of liquid particles. The role of heterogeneous chemistry on the air pollution problems of concern is well studied in a few cases, including the role of polar stratospheric clouds described in Section 5.3. However, much is still unknown.

Several studies have been published (Dentener et al., 1996, Jacob, 2000) that compile current information on heterogeneous reactions and on their impacts on tropospheric pollutants. These reactions include the hydrolysis of N_2O_5 (g), the hydrolysis of NO_2 and NO_3, and conversion of HO_2 to H_2O_2 (which may also be catalyzed by transition metal ions). In addition, there are proposed reactions for O_3 loss on soot surface and in cycles involving bromine and chlorine radicals. Reactions on mineral aerosols and windblown dust may affect the conversion of SO_2 to sulfate. In some regions of the world, dust concentrations can be high enough to affect the formation of oxidants and acids, (e.g., in Japan or southern Europe). Dentener et al. found in their model simulations that heterogeneous reactions may decrease tropospheric O_3 by up to 10% because of their effect on radical balance.

3.5 Aerosol Dynamics

Aerosol dynamics refer to processes governing the formation, growth and shrinkage of particles as a function of time. Figure 3 depicts the major processes that contribute to such changes in a particle population. New particles are formed from vapor when *nucleation* takes place. Nucleation involves a phase transition from the gas phase to the particle phase and increases the number of particles, as well as the total particle mass. Typically, new particles formed by nucleation are "ultra fine," in the diameter range of 1 to 10 nm diameter. Homogeneous nucleation occurs when a pure component particle is formed, for example, when the vapor phase is saturated. Heterogeneous nucleation occurs when gaseous molecules of different identities nucleate. Molecules in the gas phase can also *condense* onto an existing particle, increasing its size (but not the total number of

particles). Therefore, nucleation and condensation compete as a gas reaches its saturation vapor pressure. If the concentration of existing particles is high, condensation onto existing particles will prevail. Nucleation is only important in cases where the existing particle concentration is relatively low, and/or the rate of formation of condensing molecules is very high (Wexler et al., 1994). *Evaporation* is the reverse process of condensation, when a particle shrinks. Condensation and evaporation processes control the formation of secondary PM relevant for air quality. Equilibrium between the particulate phase and the gas phase occurs at the surface of the particle. The effect of particle size on equilibrium can also be taken into account to refine the treatment of gas/particle conversion at the surface. This so-called Kelvin effect limits the condensation of gases on particles as the particle size decreases. In addition, the mass transfer of molecules between the bulk phase of the gas and the surface of the particle must also be taken into account, especially for larger particles, where the kinetic transfer may actually limit the rate of condensation and evaporation. Finally, when two particles collide, they may stick to one another and *coagulate* to form a bigger particle, decreasing the total number of particles. Coagulation rates increase as the concentrations of particles increase. At PM concentrations typical of urban and regional atmospheres, coagulation is typically slow enough relative to the other processes affecting the particle size distribution that coagulation can be neglected (Seigneur and Barnes, 1986; Wexler et al., 1994).

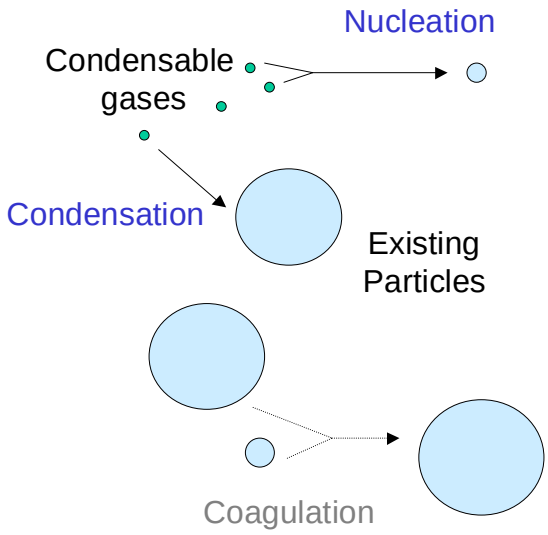

Figure 3. Processes that change the size of a particle.

4 Chemical Transformations Involved in the Formation of Air Toxics

Toxic compounds include a myriad of organic and inorganic compounds that are typically regulated in terms of their potential risk to the human population or wildlife rather than in terms of their ambient concentrations. Organic toxic

compounds include volatile organic compounds (VOC) such as benzene, 1,3-butadiene, and formaldehyde and semi-volatile organic compounds (SVOC) such as polychlorinated dibenzo-p-dioxins and polychlorinated dibenzofurans (PCDD/F), polychlorinated biphenyls (PCB), polycyclic aromatic hydrocarbons (PAH), and several pesticides, herbicides and fungicides. Inorganic toxic compounds include metals that can reside primarily in the particulate phase (e.g., arsenic, lead, chromium) or the gas phase (e.g., mercury, selenium), inorganic gases such as chlorine (Cl_2), hydrochloric acid (HCl) and hydrofluoric acid (HF) and radionuclides such as radon. We will discuss below the atmospheric chemistry of some of these toxic compounds. Radionuclides are not discussed here.

4.1 Inorganic Toxic Compounds

4.1.1 Trace Metals

The toxicity of most trace metals is not a function of their chemical speciation and, consequently, their chemical transformations are generally not relevant. Two major exceptions are chromium (Cr) and mercury (Hg). Cr exists in two valence states in the atmosphere: hexavalent, Cr(VI), and trivalent, Cr(III). Cr(VI) is considered to be carcinogenic whereas Cr(III) is not (IRIS, 2001). It is, therefore, essential to assess the valence of Cr in the atmosphere. Hg also exists in two valence states in the atmosphere: elemental, Hg(0), and divalent (or oxidized), Hg(II). In addition, Hg(II) can be present as gaseous species such as $HgCl_2$, as particulate species such as HgO or HgS, or as gaseous species adsorbed to atmospheric particulate matter. These various Hg species have different atmospheric lifetimes ranging from a few hours to about one year (Schroeder and Munthe, 1998). Therefore, it is necessary to take into account the transformations among these Hg species to properly simulate their atmospheric behavior including the relevant source-receptor relationships.

Figure 4 depicts the atmospheric chemistry of Cr (Seigneur and Constantinou, 1995). Chemical transformations between Cr(VI) and Cr(III) take place in aqueous particles or cloud/fog droplets. Cr(VI) can be reduced to Cr(III) by several chemicals including trivalent arsenic, divalent iron, vanadium and sulfur dioxide. Cr(III) can be oxidized to Cr(VI) by reactions with trivalent or tetravalent manganese. Computer simulations that have been conducted for a wide range of plausible atmospheric conditions suggest that typical conditions favor the reduction of Cr(VI) to Cr(III). Only under some extreme conditions could Cr(III) be oxidized to Cr(VI).

Figure 5 depicts the atmospheric transformations of Hg (Lin and Pehkonen, 1999; Ryaboshapko et al., 2001). The oxidation of Hg(0) to Hg(II) can occur both in the gas phase and the aqueous phase (i.e., cloud or fog droplets). However, except for the aqueous oxidation of Hg(0) by dissolved Cl_2 in marine environments, those reactions are relatively slow on average (half-life of a few months).

Reductions of Hg(II) can take place in the aqueous phase by reaction with dissolved SO_2 and HO_2 radicals. Current kinetic data suggest that the latter reaction is considerably faster and consequently dominates the conversion of Hg(II) to Hg(0) in clouds and fog during daytime. At night, oxidation of Hg(0) by Cl_2 (which can reach concentrations on the order of 100 ppt over sea water) will dominate in marine environments. Adsorption of Hg(II) to soot and other atmospheric particulate matter within droplets may inhibit Hg(II) reaction and, therefore, decrease the overall reduction rate of Hg(II) to Hg(0). At this point, it is not clear what fraction of Hg(II) gets adsorbed to particulate matter (experimental data of Seigneur et al., 1998, suggest values in the range of 9 to 55%) and to what extent their adsorption is reversible or irreversible.

4.1.2 Inorganic Gases

Non-metallic inorganic gases listed as air toxics by the U.S. Environmental Protection Agency (EPA) and the State of California include carbon disulfide (CS_2), molecular chlorine (Cl_2), hydrogen chloride (HCl), hydrogen fluoride (HF) and phosphine (PH_3). Among those, Cl_2 is very reactive and will photolyze in the presence of sunlight. The atmospheric chemistry of Cl_2 and HCl is tied to the global chlorine cycle, which includes reactions related to sea salt (Graedel and Keene, 1995; Spicer et al., 1998).

4.2 Organic Toxic Compounds

4.2.1 Volatile Organic Compounds

A myriad of VOC is listed as air toxics by the EPA, the State of California and other regulatory agencies. The toxic VOC that are considered to contribute the most to cancer risk in urban locations include benzene, 1,3-butadiene, formaldehyde, and acetaldehyde. These compounds exhibit a wide range of atmospheric chemical behavior. The reactivity of benzene is quite low (atmospheric lifetime of a few days). On the other hand, 1,3-butadiene is fairly reactive (atmospheric lifetime of about a few hours in a polluted urban environment) and the two aldehydes are primary as well as secondary and are quite reactive (atmospheric lifetimes of a few hours in a polluted urban environment). The reactive species are involved in O_3 formation as discussed in Section 2. Therefore, the assessment of such air toxics requires a full treatment of VOC atmospheric chemistry.

4.2.2 Semi-Volatile Organic Compounds

Several SVOC are listed as air toxics, including PCDD/F, PCB, PAH, and several pesticides, herbicides and fungicides. All organic compounds that contain H atoms react with OH radicals in the atmosphere. Organic compounds that contain double and triple bonds, and certain nitrogen-containing compounds react with NO_3 and O_3. In addition, organosulfur compounds and phenolic compounds react with NO_3 (Atkinson, 1994, 1996, 2000). However, the atmospheric lifetime of

most SVOC is typically on the order of a few days and they are, therefore, subject to long-range transport. The reactivity of SVOC tends to decrease with increasing number of halogen atoms. The partitioning of SVOC between the gas phase and the particulate phase also affects their reactivity. It is generally assumed that the particulate fraction is non-reactive, however, experimental evidence is currently insufficient to assess whether this is actually the case. Some SVOC may also be subject to photolysis, however, experimental data are typically not available to quantify their photolytic rates (Franklin et al., 2000).

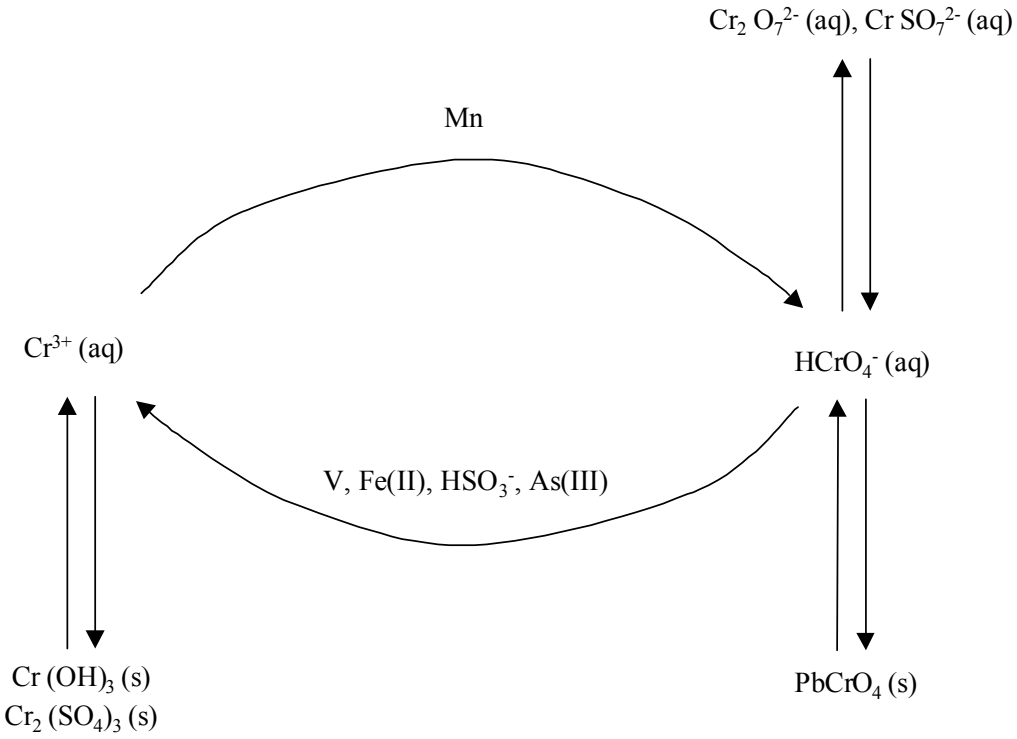

Figure 4. Condensed description of the atmospheric chemistry of chromium (Seigneur and Constantinou, 1995). (Reprinted with permission from ACS).

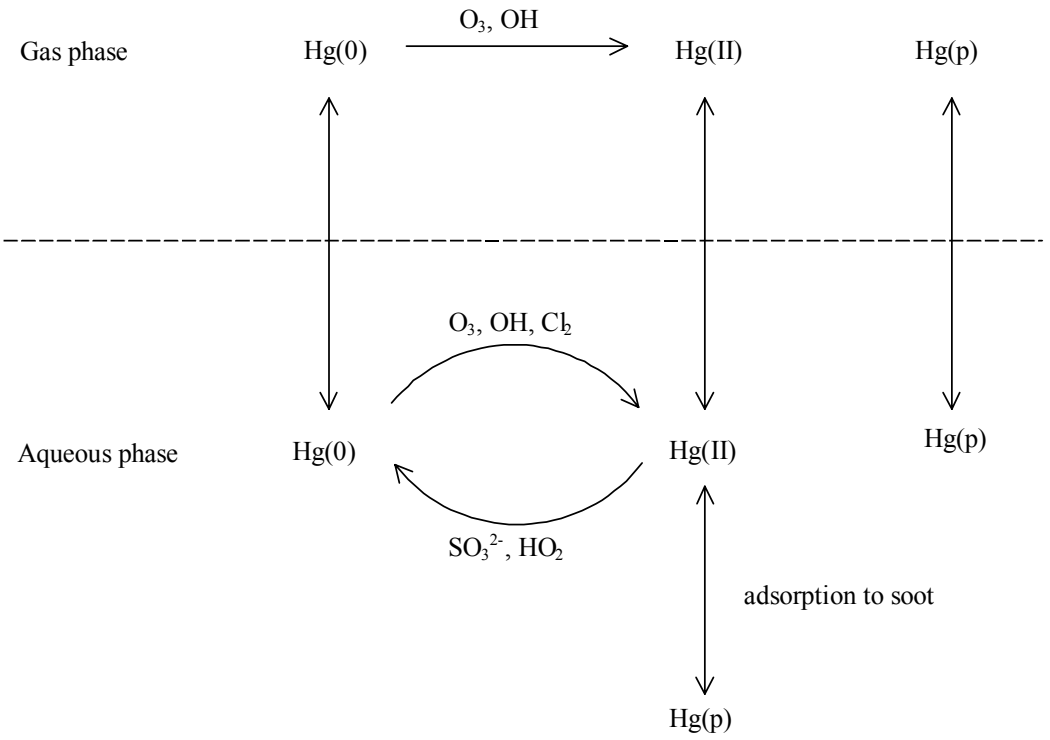

Figure 5. Condensed description of the atmospheric chemistry of mercury (after Ryaboshapko et al., 2001). (Reprinted with permission from ACS).

5 Chemistry of the Upper Atmosphere: Stratospheric Ozone

5.1 Ozone Abundance and Distribution

One of the most pressing, long-standing, and extensively studied global atmospheric issues is the gradual decline in stratospheric ozone (O_3). This decline is particularly noticeable in the lower stratosphere. Although the photochemistry and the meteorology that control the abundance and distribution of stratospheric O_3 have been investigated in great detail over the past several decades, the observations are not always well reproduced by 2-D and 3-D atmospheric models.

O_3 is produced in the stratosphere predominantly via a 2-step process initiated by the UV photolysis of molecular oxygen (Chapman, 1930),

$$O_2 + h\nu \rightarrow 2O \tag{26}$$

$$O + O_2 + M \rightarrow O_3 \tag{27}$$

Contrasting these reactions with Reactions 1 and 2 in the troposphere, O_3 is produced the same way, but the source of the oxygen atom is different. NO_x is not abundant in the stratosphere and energy-rich photons needed to dissociate O_2

are not as available in the lower atmosphere. In the stratosphere, O_3 is destroyed by photolysis and oxygen atom recombination (among a number of other mechanisms discussed below),

$$O_3 + h\nu \rightarrow O_2 + O \tag{28}$$

$$O + O_3 \rightarrow 2O_2 \tag{29}$$

Reactions 27 and 28 lead to rapid inter-conversion between odd-oxygen species O and O_3, whereas Reactions 26 and 29 generally control the net production rates of odd oxygen, and thus O_3, throughout the stratosphere. The vertical distribution of O_3 shown in Figure 6 is largely maintained by this set of reactions, known as the Chapman mechanism.

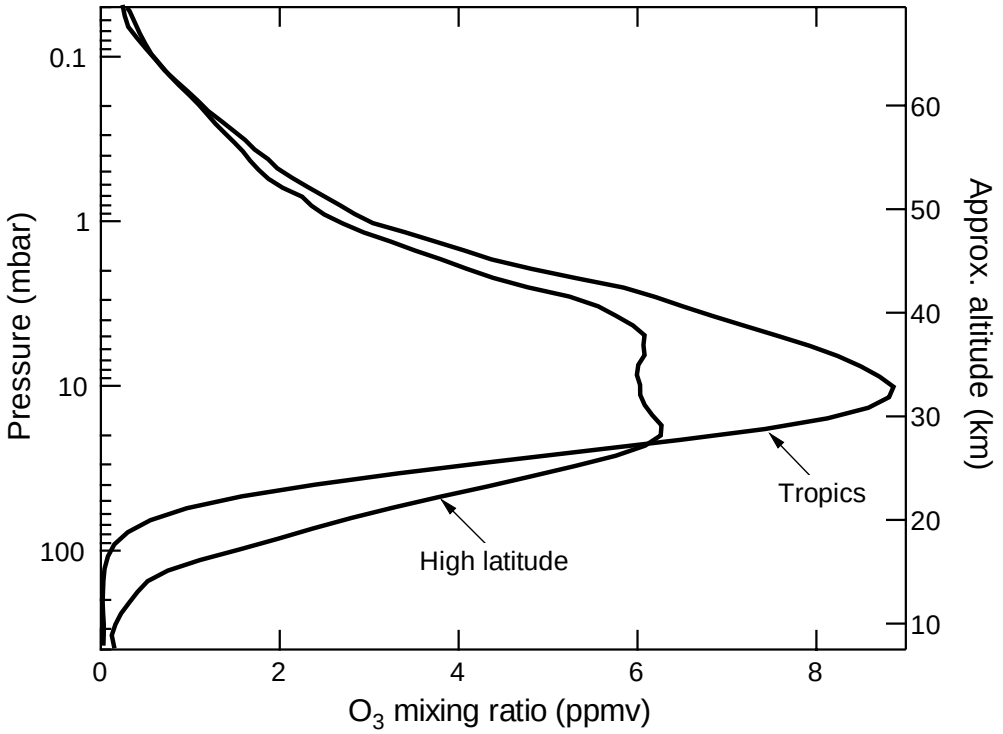

Figure 6. Vertical distribution of stratospheric O_3 at low and high latitudes. O_3 volume mixing ratios are shown as a function of pressure. The approximate altitude is shown for reference. Data were recorded at high southern latitudes and in the tropics by the space-shuttle-borne Atmospheric Trace Molecule Spectrometer (ATMOS) in November 1994.

Below ~30 km the photolysis rate of O_2 increases approximately exponentially with increasing altitude (DeMore et al., 1997), which is responsible for the steep gradient in O_3 abundance with altitude in the lower stratosphere. In the middle and upper stratosphere, O_2 photolysis is less altitude dependent, and the O_3 abundance decreases with altitude as temperature (and hence the rate constant of

Reaction 29) increases while pressure (and thus the rate of Reaction 27) continues to decrease.

This simple set of reactions, however, does not fully explain the spatial distribution of O_3 in the stratosphere. In the lower stratosphere, where the instantaneous photochemical lifetime of odd oxygen is in the range of months to years, the O_3 distribution is strongly influenced by transport processes (e.g., Brasseur and Solomon, 1986). For instance, although solar exposure and thus production rates of O_3 are highest in the tropical middle stratosphere, column abundances of O_3 are higher at higher latitudes where the peak in the vertical distribution shifts to lower altitudes. The primary large-scale stratospheric circulation pattern responsible for this redistribution of O_3 is referred to as Brewer-Dobson circulation and is characterized by average upward flow at low latitudes and outward and downward flow at higher latitudes (Dobson, 1929).

5.2 Ozone Depletion via Gas-Phase Chemistry

In addition to the dynamics and chemical mechanisms described above, there are a large number of other processes that influence O_3 abundance and distribution. O_3 can be destroyed, for example, via gas-phase catalytic cycles involving free radical oxides of hydrogen (H, OH, and HO_2) (Bates and Nicolet, 1950; Crutzen, 1971; Johnston, 1971), nitrogen (NO and NO_2) (Crutzen, 1971; Johnston, 1971), chlorine (Cl, ClO, ClO_2) (Molina and Rowland, 1974; Stolarski and Cicerone, 1974), and bromine (Br, BrO) (Wofsy et al., 1975). Iodine oxide radicals may also destroy O_3, but the stratospheric abundance of iodine is too low to have a significant effect on O_3 abundance (Solomon et al., 1994). These cycles can be described by the general form

$$X + O_3 \rightarrow XO + O_2 \tag{30}$$

$$XO + O \rightarrow X + O_2 \tag{31}$$

where X represents H, OH, NO, Cl, or Br. There are additional important cycles that involve more than one radical family, e.g. (McElroy et al., 1986),

$$Cl + O_3 \rightarrow ClO + O_2 \tag{32}$$

$$Br + O_3 \rightarrow BrO + O_2 \tag{33}$$

$$BrO + ClO \rightarrow ClO_2 + Br \tag{34}$$

$$ClO_2 + M \rightarrow Cl + O_2 \tag{35}$$

One of the more notorious O_3 loss mechanisms is an analog of the above cycle involving the ClO dimer (Molina and Molina, 1987), i.e.,

$$2(Cl + O_3 \rightarrow ClO + O_2) \quad (36)$$

$$ClO + ClO \rightarrow Cl_2O_2 \quad (37)$$

$$Cl_2O_2 + h\nu \rightarrow ClO_2 + Cl \quad (38)$$

$$ClO_2 + M \rightarrow Cl + O_2 \quad (39)$$

Model calculations indicate that Reactions 32 to 35 are responsible for 10-30% and Reactions 36 to 39 for ~70% of the O_3 loss observed in the Antarctic lower stratospheric polar vortex during austral spring, i.e., the "ozone hole" (Jones et al., 1989; McElroy and Salawitch, 1989; Solomon et al., 1990).

In the non-polar lower stratosphere, cycles involving OH and HO_2 (HO_x) are estimated to account for 30-50% and cycles involving NO and NO_2 (NO_x) for 20-40% of net O_3 destruction (McElroy, 1982; McElroy and Salawitch, 1989). At altitudes above 21 km, stratospheric O_3 loss is predominantly attributable to cycles involving NO_x (Prather et al., 1984; McElroy and Salawitch, 1989). The contribution of chlorine radicals to O_3 depletion is also significant and increases with increasing altitude up to ~40 km (Prather et al., 1984; McElroy and Salawitch, 1989).

The influence of these reactions on middle stratospheric O_3 is particularly obvious in air masses that have been confined to high latitudes for a couple of weeks or more. When air masses are caught in anticyclone regions, O_3 mixing ratios have been observed to decrease by 20-30% at altitudes between 25 and 40 km (Manney et al., 1995). These "pockets" of low O_3 air have been attributed predominantly to O_3 destruction via cycles involving NO_x under conditions characterized by low O_3 production rates (Nair et al., 1998).

A cycle similar to those that occur in the stratosphere has been implicated in frequent episodic depletion of O_3 in the upper troposphere and in the marine boundary layer. This cycle involves HO_x species and CO, i.e.,

$$CO + OH \rightarrow H + CO_2 \quad (40)$$

$$H + O_2 + M \rightarrow HO_2 + M \quad (41)$$

$$HO_2 + O_3 \rightarrow OH + 2O_2 \quad (42)$$

In order for this mechanism to be effective for tropospheric O_3 destruction, NO_x concentrations must be low, which limits the production of O_3 associated with NO_x chemistry coupled with hydrocarbon oxidation (Kley et al., 1996), as discussed in Section 2.

5.3 Role of Heterogeneous Chemistry in Ozone Destruction

Reactions mediated by aerosol and cloud particles have a large effect on lower stratospheric O_3 abundance. One such reaction is the hydrolysis of N_2O_5 to form HNO_3,

$$N_2O_5 + H_2O\ (aerosol) \rightarrow 2HNO_3 \quad (43)$$

which plays a substantial role in limiting O_3 loss via NO_x chemistry (Cadle et al., 1975). N_2O_5 is produced at night by the following set of reactions

$$NO_2 + O_3 \rightarrow NO_3 + O_2 \quad (44)$$

$$NO_3 + NO_2 + M \rightarrow N_2O_5 + M \quad (45)$$

Although N_2O_5 is not directly involved in O_3 depletion, it can be rapidly converted to NO_x by photolysis or thermal decomposition. Nitric acid is much more stable than N_2O_5, and is thus a longer-lived reservoir for reactive nitrogen.

HCl and $ClNO_3$ act similarly as reservoirs for reactive chlorine and account for the majority of the inorganic chlorine budget under most conditions in the stratosphere. HCl is more photochemically stable than $ClNO_3$, and its abundance exceeds that of $ClNO_3$ under steady-state conditions at temperatures greater than 198 K, as shown in Figure 7. At lower temperatures, however, these species react rapidly on surfaces of sulfuric acid aerosols and polar stratospheric clouds (PSCs) to form molecular chlorine, i.e.,

$$ClNO_3 + H_2O\ (aerosol) \rightarrow HOCl + HNO_3 \quad (46)$$

$$ClNO_3 + HCl\ (aerosol) \rightarrow Cl_2 + HNO_3 \quad (47)$$

$$HOCl + HCl\ (aerosol) \rightarrow Cl_2 + H_2O. \quad (48)$$

As shown in Figure 8, the rates of these reactions increase exponentially with decreasing temperature (Sander et al., 2000), but temperatures low enough to initiate this process are generally only attained within the polar vortex during the Antarctic and Arctic winters. In the polar spring, Cl_2 is photolyzed to produce atomic chlorine, which participates in catalytic cycles involving Reactions 32 to 39, thereby leading to rapid O_3 loss (McElroy et al., 1986; Solomon et al., 1986). If temperatures are low enough, nearly all of the available inorganic chlorine within the vortex is converted from HCl and $ClNO_3$ into reactive radicals, and the vortex is described as "fully activated" (see Figure 9).

The impact of aerosols and PSCs on polar O_3 is compounded by the ability of PSCs to sequester HNO_3. These particles can grow large enough to undergo sedimentation from the stratosphere, leaving the polar vortex denitrified and

possibly dehydrated (Toon et al., 1986). Denitrification reduces the rate at which ClO recombines with NO_2 to regenerate the less destructive reservoir species $ClNO_3$ (McElroy et al., 1986). If denitrification is complete, the rate of the springtime recovery of the vortex is controlled by the rate of HCl production from the reaction of atomic chlorine with methane. This route to recovery is also taken if the vortex is depleted in O_3, in which case Reaction 32 is too slow to generate ClO for the production of $ClNO_3$ by recombination with NO_2 (see Figure 9). When O_3 is only moderately depleted, and the vortex is not significantly denitrified, active chlorine preferentially recovers into $ClNO_3$ as the vortex warms. This scenario is common in the Arctic. Under O_3-depleted and/or denitrified conditions, active chlorine is converted into HCl almost exclusively. These conditions are common in the Antarctic (Michelsen et al., 1999).

Temperatures low enough to promote Reactions 46 to 48 may be reached in the lowest part of the stratosphere near the tropopause, but inorganic chlorine concentrations are usually too low to have a significant impact on O_3 abundances in these regions. Reactions 46 to 48 may promote non-polar O_3 loss at temperatures higher than 200 K when stratospheric aerosol abundances are elevated. For example, in response to injection of volcanic sulfur following a major eruption (Hofmann and Solomon, 1989), the elevated concentrations of aerosols may be at least partially responsible for the observed loss of mid-latitude O_3 in the wake of major volcanic activity.

The corresponding reactions involving bromine species,

$$BNO_3 + H_2O\ (aerosol) \rightarrow HOBr + HNO_3 \tag{49}$$

$$HOBr + HCl\ (aerosol) \rightarrow BrCl + H_2O \tag{50}$$

have rate constants orders of magnitude larger than those of Reactions 46 to 48 at temperatures higher than ~198 K (see Figure 7; Sander et al., 2000). Low abundances of bromine in the stratosphere (currently ~1.5% of the abundance of chlorine), however, limit the contribution of these reactions to non-polar lower stratospheric O_3 loss. In the troposphere, where bromine concentrations can be high, Reactions 49 to 50 are important and have been implicated in the nearly complete depletion of O_3 in the Arctic boundary layer during spring (Fan and Jacob, 1992).

Despite extensive studies of aerosol-mediated chemistry, heterogeneous processes are not understood well to explain previous responses of lower stratospheric inorganic chlorine partitioning to elevated aerosol loading (Webster et al., 2000), and thus to predict the atmospheric response to future volcanic eruptions. These reactions are very likely to be sensitive to aerosol composition. Stratospheric aerosols have been observed to contain soot, crustal and meteoritic components, such as iron, sodium, magnesium, and calcium, in addition to sulfuric acid, nitric acid, and water (Sheridan et al., 1994; Cziczo et al., 2001). Detailed studies of the

influence of these contaminants on stratospheric aerosol-mediated chemistry have yet to be performed. Similar deficiencies exist in the understanding of the effect of phase on aerosol chemistry. Sulfuric acid aerosols may undergo transitions to several metastable phases under stratospheric conditions (Zhang et al., 1993), and a survey of rates of heterogeneous reactions for these phases has not been performed.

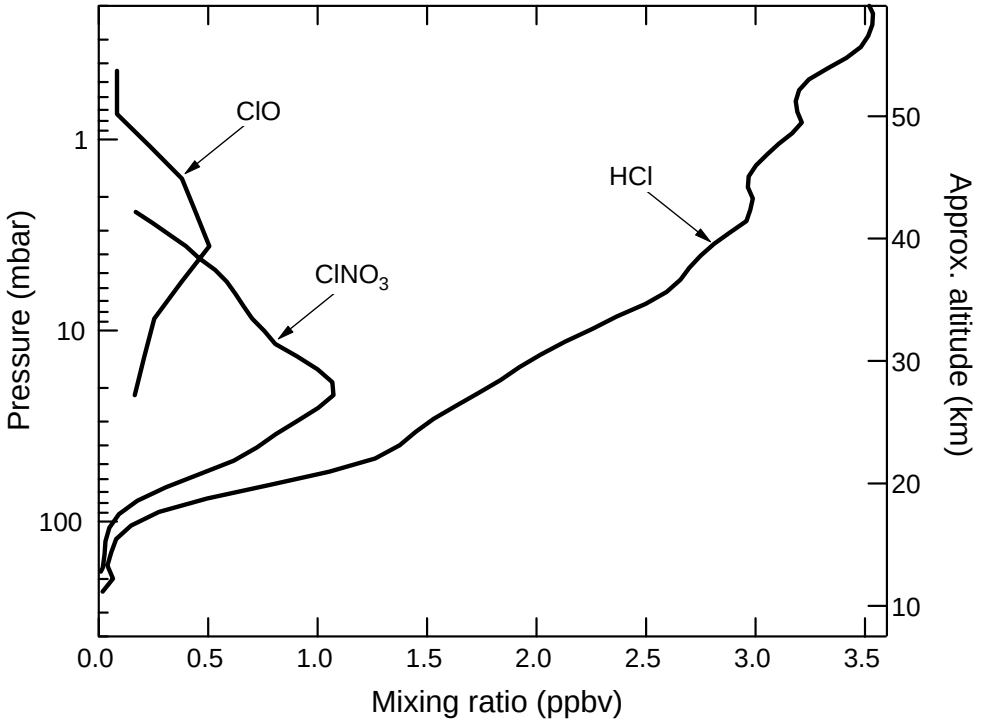

Figure 7. Vertical distributions of inorganic chlorine species. Volume mixing ratios of HCl, $ClNO_3$, and ClO are shown as a function of pressure. Data were recorded at northern mid-latitudes by ATMOS (HCl, $ClNO_3$) and the Millimeter-wave Atmospheric Sounder, MAS, (ClO) in November 1994.

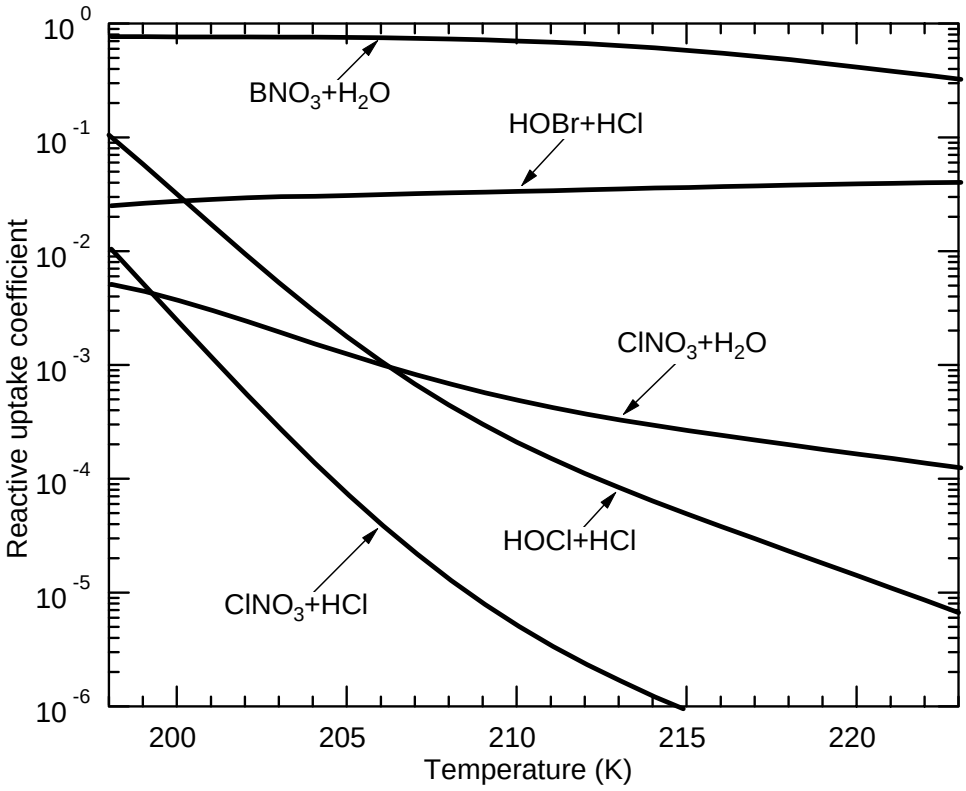

Figure 8. Temperature dependence of the reactive uptake coefficients for atmospherically important aerosol-mediated reactions. Reactive uptake coefficients (γ) for Reactions 46-50 as a function of temperature (Sander et al., 2000).

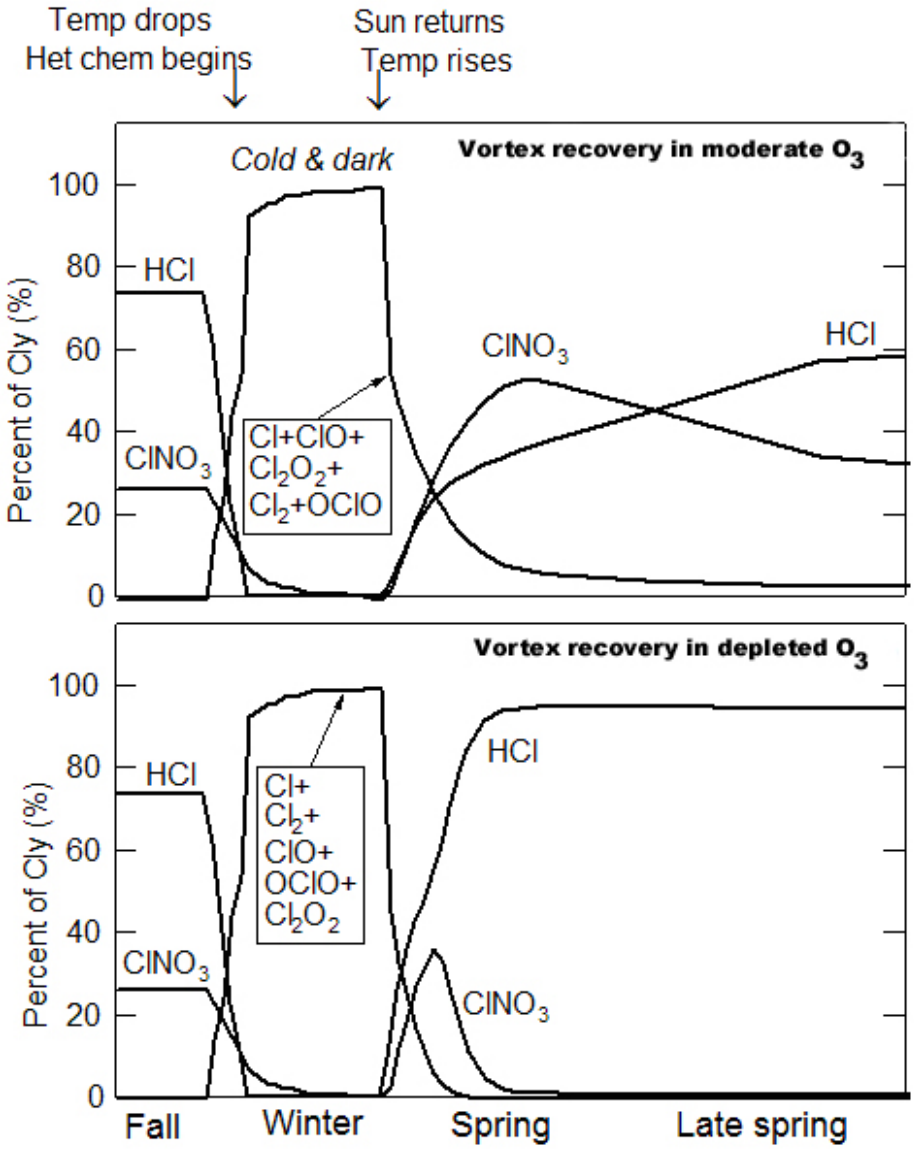

Figure 9. Evolution of the partitioning between inorganic chlorine species in the winter/springtime polar vortices. The partitioning of inorganic chlorine during the activation and recovery of the polar vortex is calculated for conditions under which O_3 is nearly completely depleted in the spring (representative of the Antarctic vortex) and only moderately depleted in the spring (more representative of the Arctic vortex). Modified from Michelsen et al. (2000) with permission from the American Geophysical Union.

5.4 Trends in Ozone and Radical Precursors

Stratospheric O_3 has been decreasing steadily for the past several decades at all extra-tropical latitudes (WMO/UNEP, 1999; Solomon, 1999; Staehilin et al., 2001 and references therein). Mid-latitude column amounts have decreased at a rate of

2-4%/decade since 1970. This decline is largest in the lower stratosphere (5-7%/decade at 15-20 km) and upper stratosphere (~7%/decade at 40 km), and is less significant in the middle stratosphere.

These trends are predominantly attributable to the increase in stratospheric abundances of chlorine and bromine. The main source of stratospheric chlorine is anthropogenic emissions of stable halogenated organic compounds, i.e., chlorofluorocarbons (CFCs) and hydrochlorofluorocarbons (HCFCs) that are not photochemically destroyed in the troposphere. Anthropogenic sources of bromine include halons and methyl bromide, although natural sources constitute a large fraction (~25%) of stratospheric abundances (Wamsley et al., 1998). These species are lofted from the troposphere into the stratosphere, where they are photolyzed to produce chlorine and bromine radicals (Molina and Rowland, 1974; Prather et al., 1984). The Montreal Protocol, originally adopted in 1987, restricts production and use of CFCs, HCFCs, halons, and methyl bromide. As a result tropospheric abundances of most of these gases have ceased to increase. Total inorganic chorine levels in the stratosphere reached a maximum in the late 1990s and are expected to decline over the next 100 years (WMO/UNEP, 1999; Solomon, 1999; Staehilin et al., 2001). Stratospheric bromine continues to increase, but its abundance is currently only 1.5% that of chlorine. Based on projections of future levels of stratospheric chlorine and bromine, and given no increases in other O_3-destroying radical precursors, O_3 is expected to recover to 1980 levels in 50-100 years (WMO/UNEP, 1999).

The major source of NO_x in the stratosphere is the oxidation of N_2O by $O(^1D)$ (Crutzen, 1971; Nevison et al., 1999). The only significant source of stratospheric N_2O is injection from the troposphere, where abundances have been increasing steadily at a rate of ~0.7 ppb/yr over the past 2-3 decades (WMO/UNEP, 1999). This trend, when extrapolated to the year 2010, is predicted to decrease middle stratospheric O_3 by at least 10% (0.5% decrease in the column amount) from present conditions (Nevison et al., 1999).

Stratospheric HO_x is predominantly generated by the reaction of H_2O with $O(^1D)$. The main sources of stratospheric H_2O are injection from the troposphere and oxidation of CH_4. The atmospheric burden of CH_4 has increased substantially over the past 200 years (Etheridge et al., 1998), and recent studies have shown that H_2O entering the stratosphere from the troposphere is also increasing. Both trends lead to increases in stratospheric humidity. Although increasing CH_4 to levels estimated for 2010 is predicted to lead to an increase in O_3 abundance throughout the stratosphere, increases in H_2O are calculated to cause a decrease in O_3 that is more substantial than the increase caused by the trend in CH_4 (Nevison et al., 1999). Projected increases in stratospheric humidity are predicted to delay the recovery of stratospheric O_3 by 10-30 years (Dvortsov and Solomon, 2001; Shindell, 2001). In addition, rates of aerosol-mediated reactions increase with increasing water vapor mixing ratios, which may have a significant effect on polar O_3 loss.

Temperatures are currently declining throughout most of the stratosphere. The mid-latitude lower stratosphere is cooling at an annual average rate of ~0.8 K/decade, and the middle and upper stratosphere are cooling at an average rate of 1-2 K/decade. The winter/springtime lower stratospheric polar vortices are cooling at ~3-4 K/decade (WMO/UNEP, 1999). The cooling trend in the lower stratosphere is primarily attributable to the downward trend in lower stratospheric O_3 abundances. Increased tropospheric greenhouse gas concentrations are at least partially responsible for the trends observed in the middle and upper stratosphere (WMO/UNEP, 1999). Trends in stratospheric humidity may also contribute to decreasing stratospheric temperatures (Dvortsov and Solomon, 2001). These trends in temperature are predicted to enhance O_3 loss and significantly decrease the rate of recovery of stratospheric O_3, particularly in the polar vortices (WMO/UNEP, 1999).

6 Modeling of Gas-Phase Chemistry

6.1 Gas-Phase Mechanisms for Ozone Formation

A chemical mechanism consists of a list of chemical reactions, like those discussed in Sections 2 through 5, with rate constants to indicate the kinetic characteristics of each reaction. The reaction rate constant, k, is most commonly a function of temperature, and may be written in the following Arrhenius form:

$$k = A \cdot exp\left(\frac{-E_a}{RT}\right) \tag{51}$$

where E_a is the activation energy, R is the universal gas constant, and T is the temperature. Two other types of reactions are included in atmospheric gas-phase mechanisms, photolysis and combination reactions. A photolysis reaction involves only one reactant, which absorbs light at some wavelengths. For a compound that absorbs light between λ_1 and λ_2, the photolysis rate constant (j) is derived as follows:

$$j = \int_{\lambda_1}^{\lambda_2} \sigma(\lambda,T)\phi(\lambda,T)I(\lambda)d\lambda \tag{52}$$

where σ is the absorption cross-section and ϕ is the quantum yield of the reaction, the probability of forming the products of interest per photon absorbed. Both σ and ϕ are properties of the light-absorbing compound and are functions of wavelength and temperature. $I(\lambda)$ is the actinic flux, which is the number of photons at a given wavelength λ. The photolysis rate constant is calculated in most applications as a discrete sum.

When two species combine to form a more stable product, some energy is typically released due to the formation of a chemical bond. Therefore, the presence of a third body facilitates this type of reaction by removing the extra energy, which otherwise may destabilize the newly formed molecule. Because of the importance of the third body stabilization effect, many combination reactions are pressure dependent.

In theory, a master mechanism may be devised that can be used to represent all the chemical reactions in the atmosphere. In practice, however, chemical mechanisms are devised to be just comprehensive enough to include all relevant processes in a particular setting. For example, the reaction of methane may not be included in many urban- to regional-scale chemical mechanisms, but can be important in global scale simulations. Similarly, radicals such as ClO (see Section 5) can be critical to the removal of stratospheric O_3, but are hardly of sufficient concentration to be of concern in the urban atmosphere. For simulating urban to regional O_3 production, chemical mechanisms are devised to represent the pertinent radical chemistry of oxygen, nitrogen, hydrogen, as well as carbonaceous compounds. However, because hundreds or thousands of VOC may be present in the ambient atmosphere, it is impractical to represent each VOC explicitly. Furthermore, the data (e.g., mechanistic and kinetic information) to support detailed mechanisms currently do not exist for many VOC. Four main strategies are currently employed to represent VOC mixtures:

- Surrogate species
- Lumped molecule
- Morphecule
- Lumped structure

In the surrogate species approach, a few VOC are represented explicitly. An entire VOC class may be represented by one of these surrogates and is assumed to react in a similar manner. This approach is especially useful in such cases as monoterpenes, where there are many compounds in the class but only a few (e.g., α-pinene, β-pinene, limonene) have been studied in detail. In the lumped molecule approach, similar compounds (e.g., long-chain alkanes) are grouped together and the reactions of the lumped molecule are devised to represent some average of all the compounds present. A new approach is to use morphecules to represent the organic mixture in the chemical solver. Each morphecule is composed of several allomorphs with different carbon numbers and reaction rates. The composition and property of each morphecule can change with time. The lumped structure approach takes into account the fact that VOC are made up of alkyl chains and functional groups. Modeled groups are chosen to represent the reactions of an alkyl group or a double bond or an aldehyde functional group, etc.

6.2 Formulating Chemical Kinetics as a Mathematical Problem

How do we turn all the mechanistic descriptions of the reactants and products and the reaction rate constants into a mathematical model that can be solved to predict the concentrations of reactants and products? Let's take a generic example:

$$\alpha_1 R_1 + \alpha_2 R_2 + \ldots \rightarrow \beta_1 P_1 + \beta_2 P_2 + \ldots \qquad k = k_1 \qquad (53)$$

where R_i are the reactants, P_j are the products, and α_i and β_j are the corresponding stoichiometric coefficients. In this case, the rate of the reaction is the product of the rate constant k_1 multiplied by the concentrations of the reactants, raised to the power of the stoichiometric coefficients:

$$r_1 = k_1 \prod_i [R_i]^{\alpha_i} \qquad (54)$$

For each reactant, the rate of change in its concentration due to this reaction is

$$\frac{d[R_i]}{dt} = -\alpha_i r_1 \qquad (55)$$

and for each product, the rate of change in its concentration is

$$\frac{d[P_i]}{dt} = \beta_i r_1 \qquad (56)$$

Note that the concentrations of the reactants decrease (negative rate of change) and the concentrations of the products increase (positive rate of change). If there is a series of N reactions, the change in concentrations of a compound, which may be a reactant in some reactions and products in other reactions, is calculated as follows:

$$\frac{d[C_i]}{dt} = \sum_{k=1}^{N} a_{ik} r_k \qquad (57)$$

where a_{ik} is the stoichiometric coefficient of compound i in reaction k. If compound i is a reactant in reaction k, $a_{ik} < 0$; if compound i is a product, $a_{ik} > 0$.

This equation is an ordinary differential equation (ODE), since the left hand side is a rate of change or a derivative in time. For each compound in the system, an ODE can be formulated. Therefore, the solution to the chemical kinetics involves the simultaneous solution to a set of ODEs, because the rates of reactions are algebraic functions of concentrations of several species. Initial conditions need to be specified for solving a set of ODEs for concentrations as a function of time.

Let us look at a special example of three reactions:

$$NO_2 + h\nu \rightarrow NO + O \qquad j_1 \qquad (58)$$

$$O + O_2 \rightarrow O_3 \qquad k_2 \qquad (59)$$

$$NO + O_3 \rightarrow NO_2 + O_2 \qquad k_3 \qquad (60)$$

There are four species involved in these three reactions. Their rates of change are:

$$\frac{d[NO]}{dt} = j_1[NO_2] - k_3[NO][O_3] \qquad (61)$$

$$\frac{d[NO_2]}{dt} = -j_1[NO_2] + k_3[NO][O_3] \qquad (62)$$

$$\frac{d[O_3]}{dt} = k_2[O][O_2] - k_3[NO][O_3] \qquad (63)$$

$$\frac{d[O]}{dt} = j_1[NO_2] - k_2[O][O_2] \qquad (64)$$

The radical (oxygen atom) is much more reactive than the other three. Since it reacts faster, the radical has a much shorter lifetime than the molecules. The concentration of the radical changes very quickly according to those of the other species in the system. Therefore, at any instant, the radical can be assumed to be in a pseudo steady state, where $\frac{d[O]}{dt} = 0$, and [O] can be solved algebraically in terms of the instantaneous concentrations of the stable species:

$$[O] = \frac{j_1[NO_2]}{k_2[O_2]} \qquad (65)$$

The pseudo steady state assumption is sometimes used in three-dimensional modeling to facilitate the solution of the system of ODEs.

By substituting Equation 65 into the system of ODEs (Equations 61 to 64), we can see that the rates of change of NO and O_3 are exactly equal in magnitude and opposite in direction to that of NO_2. Therefore, the concentrations of NO, O_3, and NO_2 will reach a steady state, called the photostationary state, where

$$[O_3] = \frac{j_1[NO_2]}{k_3[NO]} \tag{66}$$

6.3 Solvers for ODEs

The solution of the atmospheric chemical kinetic equations is a difficult task because the system of ODEs is stiff (i.e., the half-lives of the various species spans several orders of magnitude). The most accurate numerical algorithms for stiff ODEs are based on Gear's method (Gear, 1971). It is, however, computationally demanding and not suitable for large 3-D systems in its original formulation. Numerical algorithms that provide good balance for speed and accuracy for solving stiff ODEs in 3-D systems have been developed and several reviews are available on the subject (e.g., Odman et al., 1992; Dabdub and Seinfeld, 1995; Mathur et al., 1998; Jacobson, 1999).

6.4 Lagrangian/EKMA Results

6.4.1 Eulerian and Lagrangian Implementations

Photochemical schemes, such as those presented above, are used to calculate the dynamics of all photochemical species in each computational cell at each time step. In Eulerian photochemical models (e.g., McRae et al., 1982b; Tesche et a1., 1984; Carmichael et al., 1986; Ackermann et al., 1998; EPA, 1999; Jacobson, 2001a; Griffin et al., 2002), the K-theory is used to simulate atmospheric diffusion and a three-dimensional grid is superimposed to cover the entire computational domain. In the Lagrangian photochemical models, columns or walls of cells are advected according to the main wind, in a way that allows the incorporation of the emissions encountered along their trajectory. Lagrangian models also use K-theory to calculate vertical and (when available) horizontal diffusion.

The main advantage of Lagrangian models versus Eulerian ones is computational speed, which can be one to two orders of magnitude faster because of the smaller number of grid cells used in Lagrangian models versus Eulerian models[2]. Lagrangian models, however, provide concentration outputs along trajectories and, therefore, their outputs are difficult to compare with concentration measurements at fixed locations. Eulerian models are described later in this chapter.

6.4.2 The EKMA Technique

A proper elaboration of the outputs of Lagrangian photochemical models allows the use of a simple method, the so-called EKMA (Empirical

[2] The new generation of Unix workstations and PCs, however, has sharply decreased computer costs.

Kinetic Modeling Approach) technique (Dodge, 1977) to evaluate the importance of both NMHC and NO_x (and their ratio) in formulating O_3 control strategies. An example of EKMA isopleths is presented in Figure 10, in which point A illustrates a city that is characterized by an NMHCI NO_x ratio of 8:1 and a "design" value (defined as the second highest hourly O_3 measured concentration) of O_3 of 0.28 ppm. The isopleths allow the definition of different strategies to meet a certain ozone air quality standard. For example, if no change in ambient NO_x is expected and the future goal for the design value of ozone is 0.12 ppm, then the control strategy requires a progress from point A to point B in Figure 10, i.e., a reduction of NMHC by approximately 67 percent.

As seen in the example above, the EKMA method establishes, graphically, a relationship between the concentrations of ozone "precursors" (NO_x and NMHC) and the design value of ozone. Note the non-linearities in Figure 10:

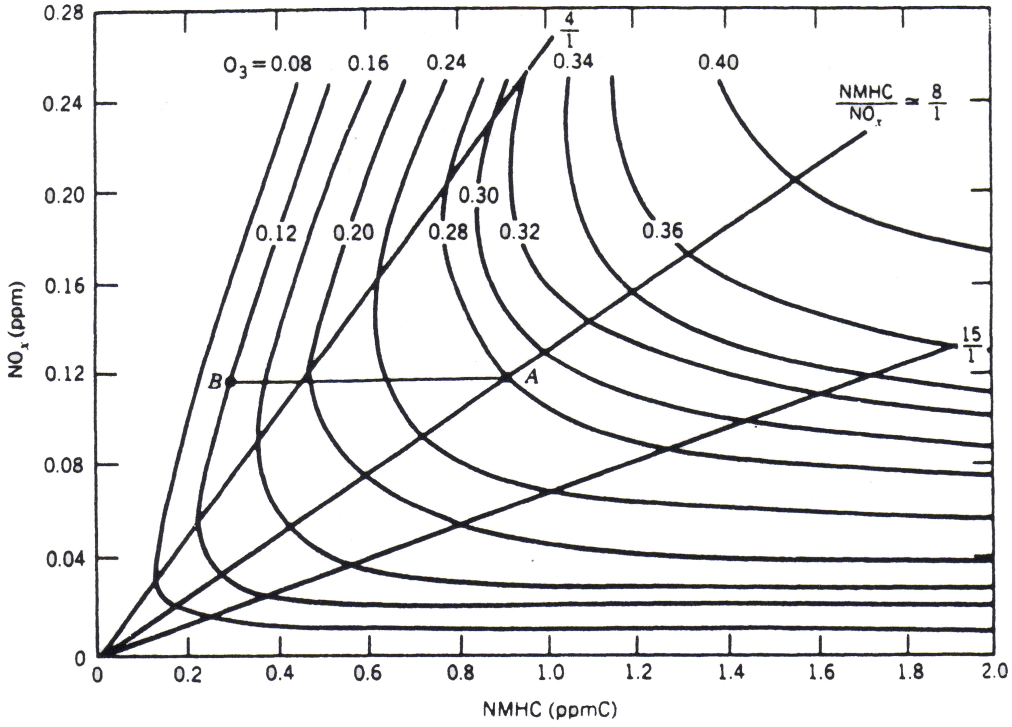

Figure 10. Ozone isopleths used in the EKMA approach (from Dodge, 1977, as presented by Finlayson-Pitts and Pitts, 1986).

EKMA isopleths should be used with caution, since they represent an oversimplified empirical description of complex nonlinear phenomena. Depending on the position of A, different emission reductions of NMHC and/or NO_x can cause both decrease and *increase* of O_3, For example, for high NMHC-to-NO_x ratios, O_3 does not vary with NHMC controls, while for low NMHC-to-NO_x ratios, NO_x controls can actually *increase* O_3. Generic isopleths in Figure 10 are

based on a series of chemical, meteorological, geographical, background and emission assumptions. A computer program, the OZIPM-2 package (Gipson, 1984) allows the generation of city-specific isopleths under conditions defined by the user.

7 Modeling of Heterogeneous and Aqueous Processes

7.1 Mathematical Modeling of Aerosol Formation

In the ambient atmosphere, particles are present in different sizes, shapes, phases, colors (light extinction properties), and composition. Each particle undergoes the processes described in Section 3.5. Therefore, one way to formulate a model would be to "follow" the development of individual particles. This is a rather cumbersome way to construct a model. Therefore, mathematical models generally follow a population of particles, which is characterized by its size distribution. This size distribution function can be expressed as number, surface area, or mass of particles in a given particle size (e.g., diameter). The area under the size distribution curve for each size range represents the number, surface area, or mass of particles in that range. Using n(v,t) to represent the continuous particle number distribution as a function of volume and time, the *general aerosol dynamics equation* is formulated as follows:

$$\begin{aligned}\frac{\partial n(v,t)}{\partial t} = & \frac{1}{2}\int_0^v K(v-\tilde{v},\tilde{v})n(v-\tilde{v},t)n(\tilde{v},t)d\tilde{v} \\ & - n(v,t)\int_{v_0}^{\infty} K(v,\tilde{v})n(v,t)n(\tilde{v},t)d\tilde{v} \\ & - \frac{\partial}{\partial v}\left[I(v)n(v,t)\right] + J_0(v)\delta(v-v_0) \\ & \left(+ S(v,t)\right)\end{aligned} \tag{67}$$

The general dynamics equation is an integral differential equation. The first two terms on the right hand side represent coagulation, where K is the coagulation coefficient as a function of the sizes of the coagulating particles. The third term represents condensation, where

$$I(v) = \Delta v(p_k - e_k) \tag{68}$$

In Equation 68, I(ν) is the rate of change of the volume of a particle of size v; Δv is the volume associated with a monomer; p_k is the frequency (s^{-1}) with which a monomer collides with a k-mer, i.e., condensation, such that the rate of condensation is defined by the product of p_k and number concentration in the particular size range; and e_k is the frequency of monomer evaporation. These processes occur at the surface of the particles, and the mass transfer of the condensing monomers from the bulk gas phase is not taken into account in the

general dynamic equation for aerosols. The fourth term in the general dynamics equation represents nucleation, at size v_0. The last term is needed in the presence of a source, S(v,t).

In practice, the range of sizes is frequently divided into a number of bins or sections. The number, surface area, or mass of particles in each section then characterizes the aerosol size distribution. This discrete representation of the particle size distribution is called the *sectional* approach. Alternately, the particle size distribution can be approximated by a series of functions characterizing different modes, e.g., lognormal distributions, and this approach is referred to as the *modal* approach.

In the simulation of particles in 3-D models, nucleation, condensation/ evaporation, and coagulation need to be modeled in conjunction with kinetic mass transfer from the bulk gas phase to the particle surface. In 3-D models, a number of computational techniques are used to facilitate the numerical simulation of particles. For example, the operator splitting approach is used to solve each term in Equation 67 sequentially. Since coagulation can typically be ignored in urban and regional atmospheres, we will focus on nucleation and condensation/evaporation in the following discussion.

7.2 Nucleation

Among the inorganic compounds of concern, sulfuric acid (H_2SO_4) has a very low vapor pressure and will preferentially reside in the particulate phase. In fact, H_2SO_4 is one of the most important nucleating species. A review of algorithms used in air quality models to predict the absolute rate of nucleation has shown that such algorithms are highly uncertain (Zhang et al., 1999). An alternative approach consists in calculating the relative rates of new particle formation and condensation (McMurry and Friedlander, 1979), and to use the new particle formation rate as a boundary condition at the lower end of the particle size distribution rather than through a detailed mechanistic representation. However, one should note that our understanding of the formation of new particles is still incomplete. Woo et al. (2001) measured the formation of new particles in various ultrafine size ranges depending on the atmospheric conditions. Formation of new particles in the 3-10 nm range is believed to be associated with the nucleation of H_2SO_4, H_2O and ammonia (NH_3) molecules (McMurry et al., 2000). However, the sources of the new particles formed in the 10-30 nm and 30-45 nm ranges are currently unknown.

Although some organic compounds are known to form new particles, e.g., products from monoterpenes (e.g., Hoffmann et al., 1998; Yu et al., 1999), the nucleation of organic compounds is not currently included in common 3-D models.

7.3 Equilibrium Partitioning of Inorganic Species

Several approaches have been used to simulate the thermodynamic equilibrium of inorganic species between the gas and particulate phases. Note that the same equilibrium relationships are used in the modeling of both aqueous particles and droplets.

7.3.1 Gas/Aqueous Partitioning

Chemical species that are soluble will partition between the gas phase and the aqueous phase. In the case of dissolution, their partitioning involves mass transfer from the bulk gas phase to the surface of the liquid droplets, thermodynamic equilibrium at the surface of the droplet (or particle) between the gas phase and the liquid phase, and mass transfer from the droplet surface to the bulk aqueous phase. The probability that a molecule that encounters the droplet surface will stick to it should also be taken into account; it is represented by the mass accommodation coefficient, α, with values ranging from 0 to 1. In the case of volatilization, these processes take place in reverse order.

The characteristic time for gas-phase diffusion is less than 10^{-2} s. The characteristic time for reaching equilibrium at the gas/droplet interface is less than 1 s for soluble gases that have an accommodation coefficient above 0.1. Characteristic times for diffusion within the droplet range from about 0.01 s for a typical cloud droplet (i.e., radius of 10 μm) to 100 s for a typical raindrop (i.e., radius of 1 mm). Therefore, mass transfer will generally not be rate limiting compared to most aqueous-phase reactions (half-lives on the order of minutes) of interest except for raindrops where aqueous-phase diffusion may become the rate-limiting step.

Thermodynamic equilibrium at the surface of the droplet can be represented by Henry's law for atmospheric trace species since their low concentrations lead to dilute solutions. The gas-phase concentrations, C_g, and the aqueous-phase concentrations, C_a, are thus related as follows.

$$H = \gamma \, C_a / C_g \tag{69}$$

where H is the Henry's law coefficient (in M/atm) and γ is the activity coefficient of the species in solution. The activity coefficient represents the fact that the droplet is not an ideal solution; it tends toward a value of unity as the solution becomes more dilute. For compounds that are not very soluble, the Henry's law constant can be estimated by the ratio of the saturation vapor pressure to the solubility - both quantities may be measured experimentally or estimated using group contribution methods.

If the liquid water content of the droplet is L (in g/m^3), then the mass balance over the gas and aqueous phases can be expressed as follows.

$$C_T = C_g \text{ x } 10^{-6} \text{ x } P / RT + C_a \text{ x } L / \rho \quad (70)$$

where C_T is the total concentration (gas-phase and aqueous-phase) in moles per m^3 of air, C_g is in ppm, C_a is in moles per liter of water (M), ρ is the density of the droplet in g/L, R is the gas constant (8.2056 x 10^{-5} m^3 atm K^{-1} mol^{-1}), T is the temperature (K) and P is the pressure (atm). Expressing C_a as a function of C_g with Equation 69 provides the gas-phase concentration as a function of C_T.

$$C_g = \frac{C_T}{10^{-6}\dfrac{P}{RT} + \dfrac{LH}{\gamma\rho}} \quad (71)$$

Similarly, the aqueous-phase concentration can be expressed as a function of the total concentration.

$$C_a = \frac{C_T}{10^{-6}\dfrac{\gamma P}{HRT} + \dfrac{L}{\rho}} \quad (72)$$

Thus, the amount of a soluble species present in cloud and fog droplets is a function of its solubility (via its Henry's law coefficient, H) and the liquid water content (L).

For a dilute solution, γ = 1, ρ = 10^3 g/L. At the surface, P = 1 atm, and the fraction of the chemical species mass present in the aqueous phase, f_a, is as follows.

$$f_a = \frac{C_a L}{C_T} = \frac{1}{\dfrac{10^{-6}}{HRTL} + 10^{-3}} \quad (73)$$

The Henry's law coefficient is a function of temperature (solubility typically increases with decreasing temperature). Values of Henry's law coefficients of major atmospheric species are available, for example, in Seinfeld and Pandis (1998), Jacobson (1999) and Finlayson-Pitts and Pitts (2000). Table 4 presents gas/liquid equilibria for selected atmospheric species.

According to Equation 73, chemical species with a Henry's law coefficient less than 400 M atm^{-1} will have less than 1% of their mass in the aqueous phase for a liquid water content of 1 g/m^3 at 298 K. Such species include O_3, NO and NO_2. The Henry's law coefficient of SO_2 is also less than 400 M atm^{-1}. However, SO_2 will dissociate in solution and it is, therefore, necessary to consider its effective

Henry's law coefficient that will include not only $SO_{2(aq)}$ but also its dissociation ions as discussed below.

7.3.2 Ionic Equilibria

Within an aqueous solution, some chemical species may dissociate into ionic forms. For example, the dissociation of $SO_{2(aq)}$ (hydrated as H_2SO_3) is represented as follows.

$$H_2SO_3 \xleftrightarrow{K_1} HSO_3^- + H^+$$

$$HSO_3^- \xleftrightarrow{K_2} SO_3^{2-} + H^+$$

where

$$K_1 = \frac{\gamma_{HSO_3^{2-}}[HSO_3^-]\gamma_{H^+}[H^+]}{\gamma_{H_2SO_3}[H_2SO_3]} \tag{74}$$

$$K_2 = \frac{\gamma_{SO_3^{2-}}[SO_3^{2-}]\gamma_{H^+}[H^+]}{\gamma_{HSO_3^-}[HSO_3^-]} \tag{75}$$

In a cloud or fog droplet, the solution is generally sufficiently dilute that the activity coefficients $\left(\gamma_{H^+}, \gamma_{H_2SO_3}, \gamma_{HSO_3^-}, \text{and } \gamma_{SO_3^{2-}}\right)$ can be assumed to be equal to one. The same is not always true for particles. Thus, the concentrations of HSO_3^- and SO_3^{2-} can be expressed as a function of $SO_{2(aq)}$ and the total concentration of dissolved SO_2 (including its ions), [S(IV)] is as follows:

$$[S(IV)] = [SO_2(aq)]\left(1 + \frac{K_1}{[H^+]} + \frac{K_1K_2}{[H^+]^2}\right) \tag{76}$$

We can then define the effective Henry's law coefficient as the ratio of the total dissolved SO_2 concentration to the SO_2 gas-phase concentration. It is related to the standard Henry's law coefficient as follows:

$$H_{SO_2,e} = H_{SO_2}\left(1 + \frac{K_1}{[H^+]} + \frac{K_1K_2}{[H^+]^2}\right) \tag{77}$$

Table 5 summarizes the ionic dissociation equilibria of SO_2 (H_2SO_3), H_2SO_4, HNO_3, NH_3 (NH_4OH), CO_2 (H_2CO_3) and H_2O. The effective Henry's law

coefficient of SO_2 at a pH of 4.5 is equal to 622 M atm^{-1}; therefore, more than 1% of SO_2 will be present in the cloud droplet for a liquid water content of 1 g/m^3.

The droplet must remain electrically neutral, that is, the positive charges of the cations must balance the negative charges of the anions. For a droplet that contains only H_2O and dissolved CO_2, the electroneutrality equation is expressed as follows.

$$[H^+] = [HCO_3^-] + 2[CO_3^{2-}] + [OH^-] \quad (78)$$

where bracket signs denote concentrations. For a CO_2 gas-phase concentration of 360 ppm, the droplet pH is 5.6. For a droplet that contains H_2O, SO_2, H_2SO_4, HNO_3, NH_3 and CO_2, this electroneutrality equation is expressed as follows.

$$[NH_4^+] + [H^+] = [HSO_3^-] + 2[SO_3^{2-}] + [HSO_4^-] + 2[SO_4^{2-}] + [NO_3^-] + [HCO_3^-] + 2[CO_3^{2-}] + [OH^-] \quad (79)$$

The concentrations of the anions and cations of the dissolved species can be expressed in terms of the total concentrations of the dissolved species (using Equation 71) and $[H^+]$ must be solved numerically via iterative techniques. Techniques frequently used include the Newton bisection method (Press et al., 1997) and others described in the next section. If one assumes that the pH is in the range of 3 to 5 (a typical range of values for most atmospheric conditions), some assumptions can be made that allow the simplification of the system to a quadratic equation for $[H^+]$ that can be solved analytically.

7.3.3 Solving Inorganic Thermodynamic Equilibria

Depending on the identities of reactants and products, the dimension of the equilibrium coefficient (K_{eq}) change. One should note that when a solid phase is involved, its activity is always assumed to be one. Several approaches are used to solve the thermodynamic equilibrium relationships. The most comprehensive approach consists in minimizing the Gibbs free energy of the multiphase system. In minimizing the Gibbs free energy, one is able to find the most stable state; this approach is, however, computationally prohibitive for explicit incorporation into most 3-D air quality models (an alternative is to parameterize the results of pre-existing simulations and retrieve the desired values from a look-up table when running the air quality model).

A more common approach used in air quality models is to solve the system of equations describing the multiphase equilibria (see Table 3 for an example). The derivation of the equilibrium relationship from the minimization of Gibbs free energy (i.e., finding the most stable state of a system), can be found in many thermodynamics textbooks and is not discussed here.

The above principles are applicable for both aqueous particles and droplets. For any system of species, many equilibrium relationships are satisfied (see Table 3). Therefore, mathematically a system of equilibrium equations needs to be solved simultaneously. As discussed in the previous section, the system of inorganic equations may be simplified algebraically into one equation in $[H^+]$. However, iterative procedures are still required to solve the equations and solving the full set of equations can still be computationally demanding. Therefore, simplifications are often made to break down the entire solution domain into subdomains that can be characterized by specific chemical regimes. In each regime, certain species may be dominant so that the less important species can be neglected without introducing significant errors into the solution. Thus, the number of equilibrium equations is reduced and the solution is obtained more rapidly.

Clearly, the number of chemical species treated in the inorganic aerosol model affects the complexity of the thermodynamic equilibrium calculations. All models treat sulfate, nitrate, ammonium and water. Some models also treat sodium and chloride to represent sea salt. Finally, the most comprehensive models also treat crustal species, i.e., magnesium, calcium, potassium and carbonate (see Zhang et al., 2000 for a comprehensive review of inorganic equilibrium modules).

7.4 Equilibrium Partitioning of Organic Species

For organic species, the first models assumed that condensable organic compounds had very low vapor pressure and consequently partition totally into the particulate phase. This is the so-called "fixed yield" approach. Later, the fixed yield model was improved to represent the saturation of organic compounds in the gas phase, and partition only the portion above saturation into the particulate phase. The saturation model was superceded by several different formulations in recent years. These include absorption, adsorption, and dissolution, as discussed in Section 3.2. One absorption formulation by Pankow (1994a, b) is used in several newer models. For compound i, the partition constant is determined as

$$K_{p,i} = \frac{A_i / TSP}{G_i} = \frac{760 RT f_{om}}{10^6 \gamma_{om,i} p^0_{L,i} MW_{om}} \tag{80}$$

where A_i is the concentration of compound i in the particulate phase (in $\mu g/m^3$ air), TSP is the total suspended particulate matter (in $\mu g/m^3$ air), G_i is the gas-phase concentration (in $\mu g/m^3$ air), R is the universal gas constant (8.2×10^{-5} m^3 atm mol^{-1} K^{-1}), T is temperature in K, f_{om} is the weight fraction of the particles that comprise the absorbing organic material phase, $p^0_{L,i}$ (torr) is the saturation vapor pressure of compound i in liquid form (sub-cooled, if necessary), $\gamma_{om,i}$ is the activity coefficient of i in mole fraction scale in the liquid phase, and MW_{om} is the

average molecular weight in the liquid phase. More recently, it has been suggested that the octanol/air partition coefficient may be used instead of $p^0_{L,i}$ as the correlating variable for the particle/air partition coefficient (Pankow, 1998) as follows:

$$K_{p,i} = K_{oa} \frac{\gamma_{oct,i}}{\gamma_{om,i}} \frac{MW_{oct} f_{om}}{10^{12} MW_{OM} \rho_{oct}} \quad (81)$$

where K_{oa} is the octanol/air partition coefficient, $\gamma_{oct,i}$ is the activity coefficient of compound i in octanol, MW_{oct} is the molecular weight of octanol, and ρ_{oct} is the density (kg m^{-3}) of octanol.

The adsorption partition constant in this case takes the following form (Pankow, 1994a,b):

$$K_{p,u} = \frac{N_s a_{tsp} T e^{(Q_l - Q_v)/RT}}{1600 p^0_{L,i}} \quad (82)$$

where N_s is the number of adsorption sites per cm^2, a_{tsp} is the surface area of the particles (m^2 g^{-1}), Q_l and Q_v are the enthalpies of desorption and volatilization (kJ mol^{-1}), and R is the universal gas constant in SI units (8.3 x 10^{-3} kJ K^{-1} mol^{-1}).

Dissolution is formulated using a regular equilibrium relationship (similar to the ammonia-ammonium equilibrium in Table 3, second row).

7.5 Treatment of Aqueous Chemistry and Multiphase Chemistry in Models

The kinetics of the oxidation of S(IV) to S(VI) by H_2O_2 is as follows (S(VI) refers to H_2SO_4 and its ions).

$$\frac{d[S(VI)]}{dt} = k_1 [H^+][H_2O_2][S(IV)] \quad (83)$$

where k_1 is in the range of 7.2 x 10^7 to 9.6 x 10^7 $M^{-2}s^{-1}$ (Lee et al., 1986; Lind et al., 1987). At pH = 4.5 and for a gas-phase H_2O_2 concentration of 1 ppb, the reaction of SO_2 with H_2O_2 is fairly rapid with a half-life of 7 s. The solubility of SO_2 is nearly inversely proportional to the concentration of H^+ (for pH above 2; see ionic equilibria above); therefore, the rate of S(VI) formation via this reaction is nearly independent of pH. Concentrations of H_2O_2 are typically on the order of a few ppb during summer months and less than 0.1 ppb during winter months in mid latitudes. However, concentrations of 1 ppb have been measured during winter in Texas, for example, as air masses from subtropical regions are transported northward (Seigneur et al., 2000).

The kinetic rate expression for the SO_2-O_3 reaction is as follows.

$$\frac{d[S(VI)]}{dt} = (k_2[H_2SO_3] + k_3[HSO_3^-] + k_4[SO_3^{2-}])[O_3] \quad (84)$$

where k_2 = 2.4 x 10^4 $M^{-1}s^{-1}$, k_3 = 3.7 x 10^5 M^{-1} s^{-1} and k_4 = 1.5 x 10^9 M^{-1} s^{-1} (Hoffmann, 1986). For an O_3 gas-phase concentration of 60 ppb and a droplet pH of 4.5, the half-life of this reaction is 46 min. As the reaction proceeds, the pH of the droplet will decrease because of S(VI) formation. The distribution of S(IV) aqueous species will shift from SO_3^{2-} toward $HSO3^-$ (see ionic equilibria above) and the reaction rate will decrease. Therefore, this reaction is self-limiting.

For a pH value around 4, the following expression is recommended for the SO_2-O_2 oxidation reaction catalyzed by Fe^{3+}.

$$\frac{d[S(VI)]}{dt} = k_5[Fe^{3+}]^2\ [S(IV)] \quad (85)$$

where k_5 = 10^9 M^{-2} s^{-1}. This reaction is also a strong function of pH. Martin (1994) provides rate expressions for this catalyzed reaction. It is most important for pH values above 5 and it is self-limiting. For example, for a concentration of 0.1 μM for Fe^{3+} and a pH of 4.5, the half-life of this reaction is 19 hours. For a pH in the range of 5 to 6, the half-life is only 12 min.

Aqueous phase chemical kinetics, like its gas-phase counterpart, involve a stiff system of ordinary differential equations. Techniques to solve stiff ODES have been discussed in Section 6.3.

8 Modeling of Reactive Plumes

8.1 Chemistry of Plumes

Plumes that contain high concentrations of NO_x (e.g., coal-fired power plant plumes) have a chemistry that differs significantly from that of the ambient background because the plume chemistry is initially VOC-sensitive and radical-limited. Therefore, the rates of formation of secondary acids such as HNO_3 and H_2SO_4 are slow as observed in power plant plumes (Richards et al., 1981; Gillani et al., 1998) and reproduced in computer simulations (Seigneur, 1982; Hudischewskyj and Seigneur, 1989; Karamchandani et al., 1998). As the plume becomes more dilute, the NO_x plume concentrations will approach the NO_x concentrations of the ambient background atmosphere. Plume chemistry will then depend on whether oxidant formation in the background atmosphere is NO_x- or VOC-sensitive.

We can distinguish three stages in plume chemistry, as summarized in Figure 12. The number of reactions needed to properly describe the plume chemistry increases from one stage to the next and also differs between daytime and nighttime. Karamchandani et al. (1998) described the chemistry of each stage. We summarize those chemical mechanisms below.

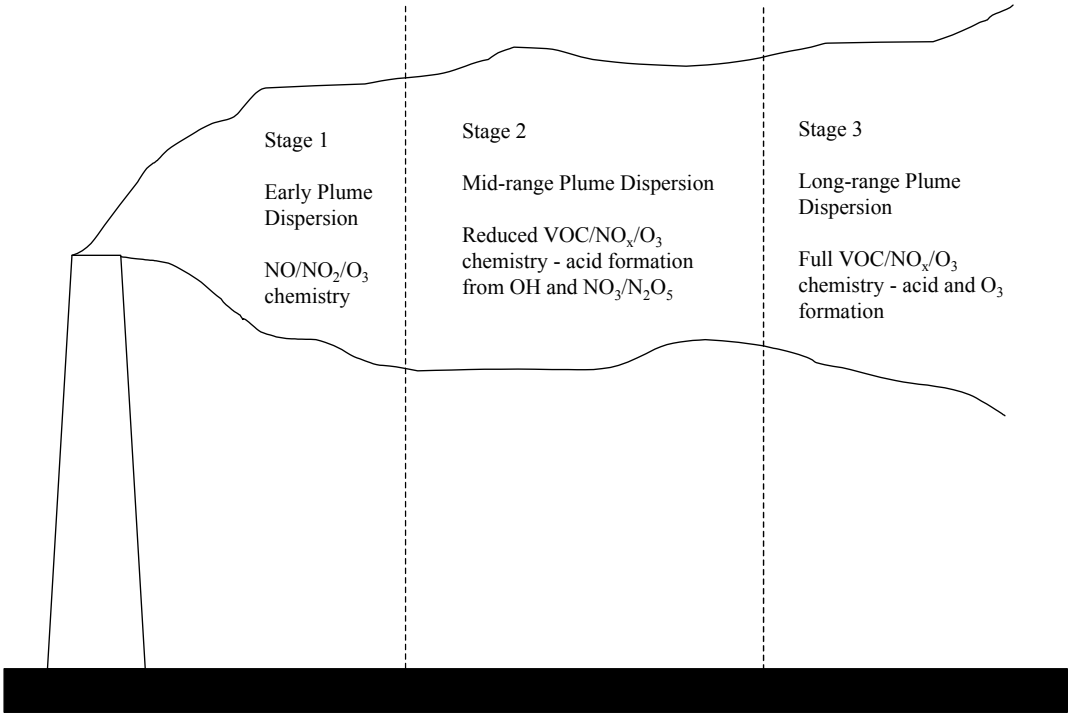

Figure 12. Schematic description of the evolution of plume chemistry with dispersion (source: Karamchandani et al., 1998; reprinted with permission from ACS).

8.1.1 Stage 1 Chemistry

Daytime.

Stage 1 corresponds to the conditions during the early stages of plume dispersion, when NO concentrations are high. During the day, the dominant reactions in this stage include four reactions among five species. This reaction set consists of the three reactions of the photostationary state between NO, NO_2 and O_3 and the termolecular oxidation of NO by O_2. This latter reaction is important very near the stack where NO concentrations are very high (i.e., above about 1 ppm). At NO concentrations of about 1 ppm, the rate of destruction of NO by O_2 is about 1%/hr. Further downwind, the oxidation of NO by O_2 becomes negligible, because its rate is proportional to the square of the NO concentration and, therefore, decreases rapidly.

Nighttime.

At night, the photolysis of NO_2 does not take place and only the oxidation reactions of NO by O_2 and O_3 need to be taken into account. Therefore, NO gets depleted and converted irreversibly to NO_2.

8.1.2 Stage 2 Chemistry

Daytime.

In Stage 2, the mid-range plume dispersion stage, reactions that form the radicals that lead to the formation of HNO_3 and H_2SO_4 must be considered. These radicals also lead to some ozone formation. However, at this stage, NO_x concentrations in the plume are significantly larger than VOC concentrations, so that O_3 concentrations within the plume are still lower than in the background air. Stage 2 daytime chemistry can be represented by the following set of reactions:

(1) The three photostationary state reactions among NO, NO_2 and O_3. Note that the termolecular oxidation of NO by oxygen can be neglected in Stage 2 once plume NO concentrations are low enough.
(2) Photolytic reactions of O_3, aldehydes, HNO_2, and H_2O_2 and the two reactions of $O(^1D)$ that lead to the formation of free radicals and, directly or indirectly, formation of OH and HO_2 radicals.
(3) Reactions corresponding to PAN chemistry and the production of radicals through PAN thermal decomposition. In the presence of high NO concentrations, PAN can be an important source of radicals.
(4) The reaction of NO with HO_2 to form NO_2 and OH, thereby converting HO_2 radicals to OH radicals, and oxidizing NO to NO_2 without O_3 consumption.
(5) The oxidation of NO, NO_2 and SO_2 to HNO_2, HNO_3 and H_2SO_4, respectively.

The differences between the daytime Stage 1 and Stage 2 mechanisms reside, therefore, in the fact that the chemistry of OH radicals is included in the Stage 2 mechanism, thereby allowing for secondary acid formation.

At this point of plume chemistry, reactions leading to O_3 formation are not important. This is apparent when comparing the rates of the oxidation reaction of NO to NO_2 by O_3 and HO_2. O_3 formation takes place when the latter reaction proceeds at a non-negligible rate, thereby producing NO_2 (which by photolysis leads to O_3 formation) without consuming O_3. In Stage 2, the ratio of the relative rates of the reactions of NO with O_3 and NO with HO_2 at the plume centerline is typically greater than 100. Therefore, in Stage 2, the reaction of NO with HO_2 is essential because it converts HO_2 to OH, but not because of its role in the conversion of NO to NO_2.

It is interesting to note that the reactions of VOC with OH contribute significantly to the consumption of OH radicals in the plume (the consumption of OH by VOC is commensurate with the reactions leading to secondary acid formation). Therefore, it may seem like VOC reactions with OH should be important. However, this is not the case because the VOC/OH reactions lead to HO_2 radicals, which are rapidly converted back to OH radicals by reaction with NO. This conversion occurs without significantly affecting the $NO/NO_2/O_3$ concentrations since these concentrations are primarily governed in Stage 2 by the photostationary state reactions, as discussed above. Moreover, the oxidation of VOC in the plume is sufficiently slower than in the background atmosphere, that it can be neglected without significantly affecting the VOC concentrations.

Nighttime.

At night, the photolysis reactions can be neglected. However, additional reactions are required to represent the formation of NO_3 radicals and N_2O_5, and the formation of nitric acid by hydrolysis of N_2O_5. The set of reactions for Stage 2 for nighttime consists of reactions that can be grouped according to the following major categories:

(1) The oxidation of NO by O_3 to form NO_2.
(2) The reactions that determine NO_3 radical concentrations, i.e., reactions of NO_2 with O_3 to form NO_3, reactions of NO_3 with NO and NO_2, subsequent formation of N_2O_5 via the latter reaction, and decomposition of N_2O_5 into its precursors.
(3) The formation of HNO_3 through N_2O_5 hydrolysis.
(4) The reactions of nocturnal PAN chemistry that lead to OH formation by reaction of NO with peroxy radicals.
(5) The formation of HNO_2, HNO_3, and H_2SO_4 by reaction of NO, NO_2 and SO_2, respectively, with OH.
(6) The radical chain termination reactions for regions of the plume where all NO has been consumed by reaction with O_3.

The differences between daytime and nighttime chemistry during Stage 2 can be summarized as follows:

(1) The lack of NO_2 photolysis at night leads to titration of NO and O_3, which will result in zero NO concentrations at the edges of the plume, and, possibly, zero O_3 concentrations at the plume core, particularly near the stack.
(2) The chemistry of NO_3 is important at night (NO_3 radicals are photolyzed rapidly during the day) and can lead to significant HNO_3 formation.
(3) In cases where background PAN concentrations are high (i.e., several ppb), its thermal decomposition in the presence of high NO concentrations leads to significant OH concentrations that are generated through reaction of NO with peroxy radicals (i.e., CH_3COO_2, CH_3O_2, and HO_2). Consequently, HNO_2, HNO_3 and H_2SO_4 formation will take place by OH oxidation of NO, NO_2 and SO_2, respectively. However, the OH

concentrations are lower during nighttime than daytime, since the photolytic reactions that generate radicals do not occur at night.

8.1.3 Stage 3 Chemistry

For dispersion of the plume at long distances where mixing with the background air has become significant, the chemistry of VOC oxidation becomes important. To simulate plume chemistry in Stage 3, a full chemical mechanism must be used.

At that point, plume chemistry will depend on whether the background atmosphere is VOC- or NO_x-sensitive for oxidant formation. If the background is NO_x-sensitive, the plume will display higher oxidant concentrations than the ambient background due to its greater NO_x concentrations; consequently, the formation of secondary acids (H_2SO_4 and HNO_3) will also occur at a faster rate in the plume than in the background. Then, as the plume becomes more dilute, plume chemistry will switch from a VOC-sensitive regime to a NO_x-sensitive regime, i.e., the rates of formation of HNO_3 and H_2SO_4 will decrease sharply and peroxides such as H_2O_2 will start forming in significant amounts in the plume. This behavior has been described via computer simulations (Karamchandani and Seigneur, 1999) as well as observed in data collected by aircraft at different downwind distances within plumes (Gillani et al., 1998). On the other hand, if the background atmosphere is VOC-sensitive for oxidant formation, the plume chemistry will tend to approach the background chemistry asymptotically and the rates of formation of H_2SO_4 and HNO_3 in the plume will approach those of the background as the plume becomes more dilute.

The explicit formulation of a chemical kinetic mechanism for these various stages of plume chemistry has been developed by Karamchandani et al. (1998) along with specific criteria based on plume and background concentrations of key species to identify the boundaries between the various stages in plume chemistry.

8.2 Gaussian Plume Models with Linear Chemistry

As described in Chapter 7A of Volume I, many plume dispersion models assume Gaussian profiles for the crosswind plume concentrations. Several of those plume models have been augmented with a simple treatment of atmospheric chemistry using first-order (i.e., linear) rate expressions. An example of such plume chemistry representation is the Mesopuff chemistry option in CALPUFF (Scire et al., 1990). As was discussed above, plume chemistry is a highly non-linear dynamic system since the VOC/NO_x ratio changes drastically as the plume becomes diluted into the background atmosphere. Therefore, plume models that use linear chemistry provide an incorrect description of plume chemistry and are unlikely to accurately simulate the concentrations of secondary pollutants such as H_2SO_4 and HNO_3 in the plume. Such models should, therefore, be used only for screening purposes.

8.3 Reactive Plume/Puff Models

Several models have been developed that combine some advanced treatment of atmospheric chemistry with a plume dispersion/transport model. Two major approaches have been used to represent plume dispersion/transport. One approach uses Lagrangian trajectories of plume cross-sections, implicitly involving the slender plume approximation. Another approach uses a population of puffs to represent the plume via their ensemble aggregation. Plume chemistry has been combined with both approaches.

Examples of reactive plume models that are based on plume cross-sections include the Reactive Plume Model (RPM) (Stewart and Liu, 1981), PLMSTAR (Hudischewskyj and Seigneur, 1989), the Panache Réactif en Atmosphère avec Dépôts (PARADE) (Joos and Seigneur, 1994), the Reactive & Optics Model of Emissions (ROME) (Seigneur et al., 1997), and the plume module of the 3-D Models-3/CMAQ modeling system (Gillani and Godowitch, 1999). All these models contain a full chemical kinetic mechanism such as CBM-IV with, in some cases, additional reactions and processes to represent secondary aerosol formation. Evaluation of model simulation results against atmospheric data collected by aircraft in plumes have shown that such reactive plume models can capture the major features of plume dispersion and chemistry, although their performance is typically severely limited by the availability of representative meteorological data (e.g., Hudischewskyj and Seigneur, 1989; Gabruck et al., 1999).

Some of the major weaknesses of plume cross-section models include their inaptitude at properly representing the effect of wind shear on plume dispersion and simulating overlapping plumes. Such limitations can be removed by using a puff modeling approach. SCIPUFF (Sykes et al., 1993; Sykes and Henn, 1995) is an example of a puff model that represents plume transport and dispersion by means of a population of puffs that expand as atmospheric turbulence dilutes their material according to the local micrometeorological characteristics. Wind shear and puff overlap are treated within SCIPUFF and more realistic representations of plume dynamics can be obtained compared to plume cross-section models. SCIPUFF has been augmented with plume chemistry and the resulting model, SCICHEM, has been evaluated against plume data (Karamchandani et al., 2000). In addition, the effect of turbulence on chemical kinetics can be simulated explicitly. This effect is more pronounced near the stack. Also, puff chemistry can be simulated in SCICHEM using the staged chemistry approach described above, in order to minimize computations.

9 Eulerian Models

Eulerian models can be used to simulate the evolution of O_3 and PM in a 3-D gridded domain. Eulerian dispersion models are described in some detail in

Chapter 10 of Volume I. In addition to dispersion and transport, which are related to the meteorological aspect of air pollution modeling, the other components for an Eulerian model include emissions (Chapter 3), chemistry (this chapter), gas/particle partitioning (this chapter), and wet and dry deposition (Chapter 13). Many Eulerian models are currently used in research and regulatory arenas. For urban to regional air quality simulations, we will list models that simulate both O_3 and PM, because PM models have the capability to simulate O_3. We will focus on the components or atmospheric transformations in these models.

9.1 Eulerian Ozone and PM Models

Table 6 lists sixteen 3-D air quality models that have been used for simulating PM in the lower troposphere. Details of twelve of these models can be found in a comprehensive review by Seigneur and Karamchandani (2001). The PM capabilities of CHIMERE, CAMx, AURAMs, and EMEP were developed since 2001, and readers will need to refer to their websites/publications for additional information. CHIMERE was developed by French organizations and is applied for air quality research, management and forecasting. CAMx is an urban/regional model that has been applied primarily in the U.S. but also in Europe. AURAMS is a new model developed by Environment Canada that is designed to treat O_3 formation, PM and acid deposition. EMEP is an Eulerian model for acid deposition and O_3 that has been upgraded to treat PM by incorporating the multicomponent monodisperse model (MULTIMONO) developed at the University of Helsinki (Pirojola and Kulmala, 2000). Another air quality model for O_3, UAM-V, is currently being upgraded for PM, but no documentation is available as of 2004 beyond the design of UAM-VPM.

Table 6. 3-D air quality models for O_3 and PM in the lower troposphere.

Model	Institution	References
CHIMERE	Ecole Polytechnique, INERIS, Université de Paris, Laboratoire d'aérologie de Toulouse	Schmidt et al., 2001; Bessagnet et al., 2004
CIT model	California Institute of Technology (Caltech)	McRae et al. (1982); McRae and Seinfeld (1983); Harley et al. (1993); Meng et al. (1998); Griffin et al. (2002)
European Acid Deposition Model (EURAD)	Ford Research Center, Germany	Hass et al., 1991, 1993, 1995, 1997; Liu et al., 1997; Langman and Graf, 1997; Ackermann et al., 1998.
Gas, Aerosol, Transport, and Radiation model (GATOR)	University of California at Los Angeles. Stanford University	Jacobson et al. (1996); Jacobson (1997b; 1997c; 2001a; 2001b); Lu et al. (1997a; 1997b).
Long Term Ozone Simulation Model (LOTOS)	TNO	Documentation in preparation

Model	Institution	References
Mesoscale Non-Hydrostatic Chemistry model (Meso-NH-C)	Centre National de Recherches Météorologiques (CNRM) and the Laboratoire d'Aérologie.	http://www.aero.obs-mip.fr/mesonh
Models-3 Community Multiscale Air Quality modeling system (Models-3/CMAQ)	U.S. EPA Office of Research & Development (ORD) Alternative versions have been developed by Atmospheric and Environmental Research, Inc. (AER) and the National Research Council of Canada	EPA, 1999; Zhang et al., 2004 www.cmascenter.org
Regional Modeling System for Aerosols and Deposition (REMSAD)	Systems Applications International (ICF-Consulting) for the U.S. EPA Office of Air Quality Planning and Standards (OAQPS)	ICF Kaiser/SAI (1999); Wayland (1999); www.remsad.com
SARMAP Air Quality Model (SAQM) with aerosols (SAQM-AERO)	State University of New York at Albany and modified for PM by the Caltech, Sonoma Technology, Inc. and others for the California Air Resources Board (CARB)	Chang et al. (1996); Dabdub et al. (1997).
Sulfur Transport Eulerian Model (STEM) Version III	University of Iowa	Zhang (1994); Carmichael et al. (1998); Song and Carmichael (1999).
Urban Airshed Model (UAM) version IV with aerosols (UAM-AERO) (UAM-IV as host air quality model)	Caltech, Sonoma Technology, Inc. and others for the California South Coast Air Quality Management District (SCAQMD) and the CARB	Lurmann et al. (1997).
UAM-AERO for long-term simulations (UAM-AERO-LT) (UAM-AERO as base model)	Sonoma Technology, Inc. for SCAQMD	Lurmann (2000).
Urban and Regional Multiscale model (URM)	Carnegie-Mellon University and the Georgia Institute of Technology	Odman and Russel, 1991b, Kumar et al. (1994); Kumar and Russell (1996a; 1996b)
CAMx	Environ International Corporation	www.camx.com
EMEP	European Monitoring and Evaluation Programme	www.emep.int/common_publications.html
AURAMS	Environment Canada	Bouchet et al. (2004)

Gas-phase chemistry. The major chemical kinetic mechanisms that are currently in use include the following:

- Carbon-Bond Mechanism IV (CBM-IV)
- The GATOR derivative of the extended CBM version
- Statewide Air Pollution Research Center mechanism (SAPRC), versions 90, 93, 97 or 99
- Regional Acid Deposition Model mechanism version 2 (RADM2)
- Regional Atmospheric Chemistry Mechanism (RACM)
- Caltech Atmospheric Chemistry Mechanism (CACM)
- Regional Lumped Atmospheric Chemical Scheme (ReLACS)
- Micro CB4

Note that a given air quality model may provide the option to use several mechanisms.

CBM-IV is based on functional groups. It includes various versions that differ in their treatment of isoprene chemistry and radical termination reactions. The most recent version (e.g., available in Models-3/CMAQ, version 2001) includes 93 reactions and 36 species. CBM-IV is also used in URM, LOTOS, SAQM-AERO, UAM-AERO, and UAM-AERO-LT. As mentioned above, the GATOR mechanism is based on the CBM formulation.

RADM2, SAPRC, RACM and CACM are based on fixed surrogate molecules for organic compounds. RACM is an updated version of RADM2. SAPRC is updated regularly and the version number corresponds to the year of the update. CACM is based primarily on RACM.

RADM2 includes 158 reactions with 57 species, and it is used in EURAD and Models-3/CMAQ. Various version of SAPRC are used in URM, STEM-III, SAQM-AERO and UAM-AERO; SAPRC99 (http://www.cert.ucr.edu/~carter) for 3-D models includes 214 reactions among 78 species. Note that as a stand-alone mechanism (box model mode), SAPRC is flexible and the user is allowed to define the number of organic species and reactions. RACM is used in STEM-III; it includes 237 reactions with 77 species. CACM is used in CIT and Models-3/CMAQ; it includes 361 reactions among 189 species (including the explicit formation of condensable organic compounds). ReLACS was developed by condensing RACM; it is used in Meso-NH-C and includes 128 reactions among 37 species.

The micro CB4 mechanism is used in REMSAD. It includes 60 reactions with a very simplified treatment of VOC chemistry using only three VOC precursors in its original formulation.

Except for CACM, all the chemical kinetic mechanisms presented here were developed for O_3 formation. Therefore, the treatment of SOA formation requires the addition of additional reactions and species.

Solvers for gas-phase chemistry. Several numerical schemes are currently used in 3-D models to solve stiff ODE systems. The major ones include Young and Boris (used in URM, Models-3/CMAQ and CIT), SMVGEAR (used in GATOR and Models-3/CMAQ), the QSSA algorithm (used in Models-3/CMAQ, EURAD, Meso-NH-C and SAQM-AERO) and the implicit-explicit hybrid (IEH) method (SAQM-AERO, UAM-AERO). Other techniques used in some of the 3-D models include the Eulerian backwards-iterative solvers used in Models-CMAQ (mechanism-specific), the column pivot method used in REMSAD, and a sparse-matrix implicit solver used in STEM-III. Some models such as Models-3/CMAQ and Meso-NH-C offer a selection of several numerical schemes. Among those solvers, SMVGEAR is the most accurate; it is however computationally more demanding although it is efficient on parallel machines. The other solvers make compromises between speed and accuracy. Our own testing of Young and Boris, QSSA and IEH suggested that Young and Boris provided the best compromise between speed and accuracy. Test results may vary however depending on the tests selected.

Aqueous and heterogeneous chemistry. The chemical kinetic mechanisms used to simulate the aqueous chemistry range from simplistic mechanisms with only one reaction (oxidation of SO_2 by H_2O_2 in REMSAD) or two reactions (oxidation of SO_2 by H_2O_2 and O_3 in Meso-NH-C) to detailed mechanisms such as the Carnegie-Mellon University (CMU) mechanism with 99 reactions, 34 equilibria and 46 species. The CMU mechanism has been incorporated into Models-3/CMAQ and a version of UAM-AERO. Other mechanisms include the Reactive Scavenging Module (RSM) mechanism used in URM that includes two reactions for the oxidation of SO_2 to sulfate, the GATOR mechanism with 64 reactions and 74 species, the mechanism of Walcek and Taylor (1986) used in EURAD and Models-3/CMAQ that includes five reactions for the oxidation of SO_2 to sulfate, and the mechanism of Möller and Mauersberer (1995) available as an option in EURAD, that includes 66 reactions among 37 species. Some models (UAM-AERO, UAM-AERO-LT and an option in REMSAD) treat aqueous-phase chemistry by arbitrarily increasing the rate of SO_2 and NO_x oxidation to sulfate and nitrate, respectively. Such parameterizations are not recommended because they fail to properly represent the nonlinear relationships between precursors and oxidation products.

Heterogeneous processes include reactions at the surface of cloud droplets and particles. The major reactions taking place at the surface of cloud droplets include the hydrolysis of N_2O_5 to HNO_3, the oxidation of NO_3 to NO_3^- and the scavenging of HO_2 to form H_2O_2. These reactions may also occur at the surface of aqueous aerosols with, in addition, the disproportionation of NO_2 to HNO_3 and HNO_2. Heterogeneous reactions at the surface of cloud droplets are generally treated as part of the bulk aqueous chemistry. Some mechanisms may, however, fail to include one of the reactions assuming that it is treated as part of the gas-phase/heterogeneous chemistry. For example, the CMU mechanism does not include the N_2O_5 hydrolysis reaction. It is, therefore, important to check that

these reactions are included in the model, either in the gas-phase or aqueous-phase mechanism.

Except for STEM-III and a recent version of Models-3/CMAQ, heterogeneous reactions at the surface of particles are not treated in the air quality models reviewed here. Such reactions may affect the formation of O_3, H_2SO_4, and HNO_3 in the presence of high concentrations of particles. For example, a simulation with heterogeneous reactions on particles showed 10% less O_3 production in the Los Angeles basin than the simulation without heterogeneous reactions.

Gas/particle partitioning of inorganic species. The partitioning of inorganic species between the gas phase and the particulate phase is governed by (1) mass transfer from the bulk gas-phase to the surface of the particle and (2) thermodynamic equilibrium of chemical species between the gas and particulate phases and within the particle. Detailed treatment of mass transfer is used only in two models, CIT and GATOR (a version of Models-3/CMAQ also includes this option but it has not been used). Some models use a hybrid approach that combines some full equilibrium assumptions with some size-distributed condensation process (e.g., UAM-AERO, Models-3/CMAQ). All the other models assume full equilibrium between the gas phase and the particulate phase.

The treatment of thermodynamic equilibrium is performed with a few major modules, most of which were reviewed by Zhang et al. (2000). These modules include the following:

- MARS-A: it uses simplifying assumptions for the sulfate/nitrate/ammonium/water system
- ISORROPIA: it uses simplifying assumptions for the same species as MARS-A with, in addition, sodium chloride (representing sea salt)
- SEQUILIB: it treats the same species as ISORROPIA but is not as accurate
- SCAPE2: it includes the same species as ISORROPIA with, in addition, potassium, magnesium, calcium and carbonate (representing soil dust)
- EQUISOLV II: it treats the same species as SCAPE2 but uses a different numerical solution procedure

MARS-A is used in Models-3/CMAQ, EURAD and LOTOS; it is also being incorporated into REMSAD, and Meso-NH-C uses a similar module. ISORROPIA is used in URM, UAM-AERO and Models-3/CMAQ. SEQUILIB was originally used in UAM-AERO and is still used in SAQM-AERO. SCAPE2 is used in CIT, STEM III and Models-3/CMAQ. EQUISOLV II is used in GATOR.

In addition, some models use parameterizations that are either based on simplifying assumptions or derived from a look-up table developed with a thermodynamic equilibrium model. Such parameterizations are used in REMSAD (as an option) and UAM-AERO-LT.

Gas/particle partitioning of organic species. The treatment of the partitioning of organic species between the gas phase and the particulate phase has evolved considerably over the past few years and the algorithms used in the various air quality models tend to reflect the time of their development. The major approaches to treating gas/particle partitioning for organic species can be summarized as follows:

- All condensable organic compounds are assumed to be in the particulate phase
- The partitioning is derived from experimental data (e.g., smog chamber experiments of Odum et al. (1996, 1997) and Griffin et al. (1999)) and is based on absorption into an organic particulate phase.
- The partitioning is based on Henry's law equilibrium for soluble organic compounds.
- The partitioning is derived from first principles and includes (1) absorption into an organic particulate phase and (2) dissolution into aqueous particles, e.g., MADRID (Pun et al., 2000, 2002).

The first approach is used in URM, STEM-III, REMSAD, SAQM-AERO, an early version of UAM-AERO, and, for some species, in GATOR. Note that REMSAD treats SOA as a fraction of the emitted VOC (i.e., there is currently no explicit treatment of SOA formation in the atmosphere; however, this is currently being revised).

The empirical partitioning approach based on absorption into an organic phase is used in Models-3/CMAQ, Meso-NH-C, UAM-AERO and UAM-AERO-LT. The solubility approach is used for some species in GATOR. The more comprehensive approach that includes both absorption into an organic phase and dissolution into aqueous particles is used in CIT and Models-3/CMAQ. EURAD and LOTOS do not treat organic aerosols.

Particle size distribution. The treatment of the particle size distribution in an air quality model falls into one of three categories:

- treatment of fine and/or coarse particles only
- treatment of the particle size distribution with a modal representation
- treatment of the particle size distribution with a sectional representation that includes more than two sections

Models that use the simple treatment of only fine and coarse particles include REMSAD and UAM-AERO-LT. Note that models that use a sectional representation (see below) can be applied with two size sections representing fine and coarse particles, respectively.

Models that use a modal representation include Models-3/CMAQ, EURAD, LOTOS, Meso-NH-C and STEM-III. Models-3/CMAQ and STEM-III treat both fine and coarse particles whereas EURAD, LOTOS and Meso-NH-C treat only fine particles.

Models that use a sectional representation with more than two size sections include URM, GATOR, SAQM-AERO, UAM-AERO, Models-3/CMAQ and CIT.

The models that use only one or two size sections only treat gas/particle partitioning but do not treat particle growth/shrinkage, coagulation and nucleation since the two sections can be assumed to be independent of each other.
Models that use a modal representation treat particle growth/shrinkage, coagulation and nucleation. However, they do not treat the kinetic mass transfer between the bulk gas phase and the particle surface.

Models that use a detailed sectional representation treat particle growth/shrinkage, may treat nucleation as a boundary condition for the lowest size section, and treat, in some cases, mass transfer (CIT and GATOR), except for GATOR, which does not treat coagulation.

9.2 Models for Toxic Air Pollutants

A comparison of five distinct Hg chemistry models developed in North America and Europe using the same data set for initialization has demonstrated that despite a common core of processes for Hg transformation processes, significant discrepancies still remain among the various existing models (Ryaboshapko et al., 2001). For example, maximum aqueous Hg(II) concentrations simulated by the five models during a 48-hour simulation ranged from 55 to 148 ng/l and minimum concentrations ranged from 20 to 110 ng/l. Although all those concentrations commensurate with available atmospheric data (e.g., Ebinghaus and Slemr, 2000), the variability among the models points out that significant uncertainties remain in our understanding of the atmospheric chemistry of Hg.

9.3 Stratospheric Models

A list of 10 two-dimensional models that contributed to the last World Meteorological Organization (WMO) ozone assessment is provided in Table 7. Seven 3-D models under development for assessment are also included.

Table 7. Two- and three-dimensional models for assessing stratospheric ozone.

2-D Model	Institution	Reference
AER	AER	Weisenstein et al. (1998)
CAM	Univ. of Cambridge, UK	Bekki, and Pyle (1994)
CSIRO	Commonwealth Scientific and Industrial Research Organization, Telecommunications and Industrial Physics, Australia	Randeniya et al. (1997)
GSFC	Goddard Space Flight Center	Jackman et al. (1996)
LLNL	Lawrence Livermore National Laboratory	Kinnison et al. (1994):

2-D Model	Institution	Reference
MPIC	Max-Planck-Institut fur Chemie, Germany	Groos, et al. (1998):
OSLO	Univ. of Oslo, Norway	Zerefos et al. (1997)
RIVM	National Institute of Public Health and the Environment, Netherlands	Law and Pyle (1993)
SUNY-SPB	State Univ. of NY at Stony Brook and Russian State Hydrometeorological Institute, St. Petersburg, Russia	Smyshlyaev and Yudin (1995)
UNIVAQ	Univ. of L'Aguila, Italy	Pitari et al. (1993)
3-D Model		
UNIVAQ	Univ. of L'Aquila, Italy	Pitari et al. (1992)
GISS	Goddard Institute of Space Studies	Rind et al. (1998)
EMERAUDE	Meteo-France Centre National de Recherches Meterosolgiques	Mahfouf et al. (1993)
Arpege/REPROBUS (ARPROBUS)	Meteo-France Centre National de Recherches Meterosolgiques	Deque and Piedelievre (1995)
ECHAM3/CHEM European Centre		Steil et al. (1998)
UKMO Mechanistic	UK Met Office	Austin et al. (1992)
UKMO Chemistry-Climate	UK Met Office	Austin et al. (1997)

9.4 Plume-in-Grid Modeling

Three-dimensional (3-D) modeling of air quality is typically based on a gridded representation of the atmosphere where atmospheric variables such as chemical concentrations are assumed to be uniform within each grid cell. Such a grid-based approach necessarily averages emissions within the volume of the grid cell where they are released. This averaging process may be appropriate for sources that are more or less uniformly distributed at the spatial resolution of the grid system. However, it may lead to significant errors for sources that have a spatial dimension much smaller than that of the grid system. For example, stack emissions lead to plumes that initially have a dimension of tens of meters, whereas the grid cell horizontal size is typically several kilometers in urban applications up to about 100 km in regional applications. This artificial dilution of stack emissions leads to (1) lower concentrations of plume material, (2) unrealistic concentrations upwind of the stack, (3) incorrect chemical reaction rates due to the misrepresentation of the plume chemical concentrations and turbulent diffusion, and (4) incorrect representation of the transport of the emitted chemicals. The errors associated with the grid-averaging of stack emissions can be eliminated by using a subgrid-scale representation of stack plumes that is imbedded in the 3-D grid system of the air quality model.

The first subgrid-scale treatment of plumes in 3-D air quality models was the Plume Airshed Reactive Interacting System (PARIS) developed by Seigneur et al.

(1983). Other treatments of subgrid-scale effects have been developed over the years (e.g., Gillani et al., 1986; Sillman et al., 1990; Morris et al., 1991; Kumar et al., 1996; Myers et al., 1996; Gillani and Godowitch, 1999). All these models treat the plume at a subgrid-scale, thereby eliminating some of the errors associated with the 3-D grid representation. However, they fail to represent the complex dispersion processes associated with the plume mixing into the background air because the plume dimensions are represented by simple geometric functions (columns, grids, ellipses, or Gaussian distributions). As discussed above, physical phenomena such as the effect of wind shear on plume dispersion, the effect of plume overlaps (e.g., under conditions of reversal flow or merging of adjacent plumes), and the effect of atmospheric turbulence on chemical kinetics are not (or poorly) represented by such models.

As described above, SCICHEM is a reactive plume model that combines an advanced treatment of plume dynamics with comprehensive atmospheric chemistry. SCICHEM is, therefore, ideally suited to simulate the subgrid-scale processes associated with the plumes of large point sources. SCICHEM has been incorporated into the 3-D Models-3/CMAQ modeling system. Its application to two distinct areas in the eastern United States (Nashville/western Tennessee and the Northeast) suggests that the treatment of large point sources such as coal-fire power plants with an advanced plume-in-grid module leads to small but non-negligible effects on O_3 concentrations and large effects on HNO_3 concentrations (and, therefore, also possibly on H_2SO_4 concentrations). For both O_3 and HNO_3, lower concentrations were simulated when the plume-in-grid treatment was used (Karamchandani et al., 2002).

References

Ackermann, I.J., H. Hass, M. Memmesheimer, A. Ebel, F.S. Binkowski and U. Shankar, 1998. Modal aerosol dynamics model for Europe: Development and first applications, *Atmos. Environ.* (32): 2981-2999.

Ames, J., T.C. Myers, L.E. Reid, D.C. Whitney, S.H. Golding, S.R. Hayes, and S.D. Reynolds. 1985a. *SAI Airshed Model Operations Manual. Vol. I: User's Manual. U.S. EPA Publication EPA-600/8-85-007b. U.S. Environmental Protection Agency*, Research Triangle Park, North Carolina. (NTIS No. PB 85-191567)

Ames, J., S.R. Hayes, T.C. Myers, and D.C. Whitney. 1985b. *SAI Airshed Model Operations Manuals. Vol. II: Systems Manual. EPA Publication EPA-600/8-85-007b. U.S. Environmental Agency*, Research Triangle Park, North Carolina.

Atkinson, R, 1997. Gas-phase tropospheric chemistry of volatile organic compounds: 1. Alkanes and alkenes. *J. Phys. Chem. Ref. Data* (26): 215-290.

Austin, J., N. Butchart, and K. Shine, 1992. Possibility of an Arctic ozone hole in a doubled-CO2 climate. *Nature* (360): 221-225.

Austin, J., N. Butchart, and R.S. Swinbank, 1997. Sensitivity of ozone and temperature to vertical resolution in a GCM with coupled stratospheric chemistry. *Q.J.R. Meteor. Soc*. (123): 1405-1431.

Bates, D. R., and M. Nicolet,1950. The photochemistry of atmospheric water vapor. *J. Geophys. Res.* (55):301-327.

Bekki, S., and J.A. Pyle, 1994. A two-dimensional modeling study of the volcanic eruption of Mount Pinatubo. *J. Geophys. Res*. (99):18,861-18,869.

Berntsen, T.J., S. Karlsdottir and D.A. Jaffe, 1999. Influence of Asian emissions on the composition of air reaching northwestern United States, *Geophys. Res. Lett.* (26): 2171-2174.
Bessagnet, B., A. Hodzic, R. Vautard, M. Beekmann, S. Cheinet, C. Honoré, C. Liousse and Laurence Rouil, 2004. Aerosol modeling with CHIMERE – preliminary evaluation at the continental scale, *Atmos. Enviro*n., (38): 2803-2817.

Brasseur, G., and S. Solomon, 1986. *Aeronomy of the Middle Atmosphere*. Dordrecht: D. Reidel.

Boucher, V.S., M.D. Moran, L.P. Crevier, A.P. Dastoor, S. Gong, P.A. Makar, S. Menard, B. Pabla, L. Zhang, 2004. Wintertime and summertime evaluation of the regional PM air quality model AURAMS. In air Pollution Modelling and Its Application XVI, C. Borrego and S. Incecik, Editors, Kluwer/Plenum Publishers, New York, 97-104.

Cadle, R. D., P. Crutzen, and D. Ehhalt, 1975. Heterogeneous chemical reactions in the stratosphere. *J. Geophys. Res.* (80): 3381-3385.

Carmichael, G.R., L.K. Peters, and T. Kitada. 1986. A second generation model for regional scale transport/chemistry/deposition. *Atmos. Environ.*, (20):173-188.

Carmichael, G.R., I. Uno, M.J. Phadnis, Y. Zhang and Y. Sunwoo, 1998. Tropospheric ozone production and transport in the springtime in east Asia, *J. Geophys. Res*, (103): 10649-10671.

Chang, J.S., S. Jin, Y. Li, M. Beauharnois, K-H. Chang, H-O. Huang, C-H. Lu, G. Wojcik, S. Tanrikulu and J. DaMassa, 1996. The SARMAP Air Quality Model. Part 1 of SAQM *Final Report. California Air Resources Board*, Sacramento, California.

Chapman, S., 1930. On ozone and atomic oxygen in the upper atmosphere. *Philos. Mag.* (10):369-383.

Crutzen, P. J., 1971. Ozone production rates in an oxygen-hydrogen-nitrogen oxide atmosphere. *J. Geophys. Res.* (76):7311-7327.

Cziczo, D. J., D. S. Thompson, and D. M. Murphy, 2001. Ablation, flux, and atmospheric implications of meteors inferred from stratospheric aerosol. *Science* (291):1772-1775.

Dabdub, D. and J.H. Seinfeld, 1995. Extrapolation techniques used in the solution of stiff ODEs associated with chemical kinetics of air quality models, *Atmos. Environ.* (29): 403-410.

Dabdub, D., L.L. DeHaan, N. Kumar, F. Lurmann and J.H. Seinfeld, 1997. Computationally efficient acid deposition model for California, *Draft Report, California Air Resources Board,* Sacramento, California.

Dachs, J. and S.J. Eisenrich, 2000. Adsorption onto aerosol soot carbon dominates gas-particle partitioning of polycyclic aromatic hydrocarbons, *Environ. Sci. Technol.* (34): 3690-3697.

DeMore, W. B., S. P. Sander, D. M. Golden, R. F. Hampson, M. J. Kurylo, C. J. Howard, A. R. Ravishankara, C. E. Kolb, and M. J. Molina, 1997. *Chemical Kinetics and Photochemical Data for Use in Stratospheric Modeling, Evaluation number 12*. JPL Publication 97-4, Pasadena, California.

Dentener, F.J., G.R. Carmichael, Y. Zhang, J. Lelieveld, P.J. Crutzen, 1996. Role of mineral aerosol as reactive surface in the global troposphere, *J. Geophys. Res.* (101): 22869-22889.

Deque, M., and J.P. Piedelievre, 1995. High resolution climate simulation over Europe. *Clim. Dyn*. (11): 321-339.

Dobson, G. M. B., 1929. Measurements of the amount of ozone in the Earth's atmosphere and its relation to other geophysical conditions. *Proc. R. Soc. London, Ser. A* (122):456-486.

Dodge, M. C. 1977. Combined use of modeling techniques and smog chamber data to derive ozone-precursor relationships. Proceedings, *International Conference on Photochemical Oxidant Pollution and Its Control*, Vol. II, edited by B. Dimitriades, *U.S. Environmental Protection Agency Document EPA-600/3-77-001b*, pp. 881-889.

Dvortsov, V. L., and S. Solomon, 2001. Response of the stratospheric temperatures and ozone to past and future increases in stratospheric humidity. *J. Geophys. Res.* (106): 7505-7514.

Ebinghaus, R. and F. Slemr, 2000. Aircraft measurements of atmospheric mercury over southern and eastern Germany, *Atmos. Environ.* (34): 895-903.

EPA, 1999. Science Algorithms of the EPA Models-3 Community Multiscale Air Quality (CMAQ) Modeling System, *EPA/600/R-99/030, Office of Research and Development, U.S. Environmental Protection Agency*, Washington, D.C.

Etheridge, D. M., L. P. Steele, R. J. Francey, and R. L. Langenfelds, 1998. Atmospheric methane between 1000 A.D. and present: Evidence of anthropogenic emissions and climate variability. *J. Geophys. Res.* (103):15,979-15,993.

Fan, S.-M., and D. J. Jacob, 1992. Surface ozone depletion in Arctic spring sustained by bromine reactions on aerosols. *Nature* (359):522-524.

Finlayson-Pitts, B.J., and J.N. Pitts, Jr. 1986. *Atmospheric Chemistry: Fundamental and Experimental Techniques*. New York: John Wiley.

Finlayson-Pitts, B.J. and J.N. Pitts, 2000. *Chemistry of the Upper and Lower Atmosphere*. Academic Press, San Diego, CA.

Franklin, J., R. Atkinson, P.H. Howard, J.J. Orlando, C. Seigneur, T.J. Wallington, C. Zetzsch. 2000. Chapter 2: Quantitative determination of persistence in air, pp. 7-62, in *Persistence and Long-range Transport of Organic Chemicals in the Environment*, G. Klecka et al., eds., Society for Environmental Toxicology and Chemistry, Pensacola, FL.

Gabruck, R.S., R.I. Sykes, C. Seigneur, P. Pai, P. Gillespie, R.W. Bergstrom, P. Saxena, 1999. Evaluation of the reactive and optics model of emissions (ROME), *Atmos. Environ.* (33): 383-399.

Gear, C.W., 1971. *Numerical Initial Value Problems in Ordinary Differential Equations*, Prentice-Hall, Englewood Cliffs, New Jersey.

Gillani, N.V., J.F. Meagher, R.J. Valente, R.E. Imhoff, R.L. Tanner, M. Luria, 1998. Relative production of ozone and nitrates in urban and rural power plant plumes 1. Composite results based on data from 10 field measurement days, *J. Geophys. Res.* (103): 22593-22615.

Gillani, N.V. and J.M. Godowitch, 1999. Plume-in-grid treatment of major point source emissions, Chapter 9 in Byun and Ching, EPA, 1999, *op. cit.*

Gipson, G.L. 1984. *User's manual for OZIPM-2: Ozone isopleth plotting with optional mechanisms/Version 2. U.S. Environmental Protection Agency Document EPA-450/4-84-024, Office of Air Quality Planning and Standards, Monitoring and Data Analysis Division*, Research Triangle Park, North Carolina.

Graedel, T.E. and W.C. Keene, 1995. Tropospheric budget of reactive chlorine, *Global Biogeochem. Cycles* (9): 47-77.

Griffin, R.J., D.R. Cocker III, R.C. Flagan and J.H. Seinfeld, 1999. Organic aerosol formation from the oxidation of biogenic hydrocarbons, *J. Geophys. Res.* (104) 3555-3567.

Griffin, R.J., D. Dabdub, M.J. Kleeman, M.P. Fraser, G.R. Cass and J.H. Seinfeld, 2002. Secondary organic aerosol: III. Urban/regional scale model of size- and composition-resolved aerosols, *J. Geophys. Res.* (107): 101029/2001JD000544.

Groos, J.-U., C. Bruhl, and T. Peter, 1998. Impact of aircraft emissions on tropospheric and stratospheric ozone: Part I, Chemistry and 2-D model results. *Atmos. Environ*. (32) 3173-3184.

Harley, R.A., A.G. Russell, A.G., G.J. McRae, G.R. Cass and J.H. Seinfeld, 1993. Photochemical modeling of the Southern California Air Quality Study, *Environ. Sci. Technol*. (27): 378-388.

Hass, H., R.J. Jakobs, M. Memmesheimer, A. Ebel and J.S. Chang, 1991. Simulation of a wet deposition case in Europe using the European acid deposition model (EURAD), *Air Pollution Modeling and Its Application VIII*, H. van Dop and D.G. Steyn, eds., 205-213, Plenum Press, New York.

Hass, H., A. Ebel, H. Feldmann, H.J. Jakobs and M. Memmesheimer, 1993. Evaluation studies with a regional chemical transport model (EURAD) using air quality data from the EMEP monitoring network, *Atmos. Environ.* (27A): 867-887.

Hass, H., M. Memmesheimer, H. Jakobs and A. Ebel, 1995. Analysis of ozone and precursor budget over Europe as simulated by the Regional Air Quality Model EURAD, in *Regional Photochemical Measurement and Modeling Studies*, A.J. Ranzieri & P.A. Solomon, eds., 934-943, Air & Waste Management Association, Pittsburgh, Pennsylvania.

Hass, H., P.J.H. Builtjes, D. Simpson and R. Stern, 1997. Comparison of model results obtained with several European regional air quality models, *Atmos. Environ.* (31): 3259-3279.

Health Effects Institute, 2001. Airborne *particles and health: HEI epidemiologic evidence*: www.healtheffects.org.

Hofmann, D. J., and S. Solomon, 1989. Ozone destruction through heterogeneous chemistry following the eruption of El Chichón. *J. Geophys. Res.* (94): 5029-5041.

Hoffmann, T., R. Bandur, U. Marggraf, M. Linscheid, 1998. Molecular composition of organic aerosols formed in the α-pinene/O_3 reaction: implications for new particle formation processes, *J. Geophys. Res.* (103): 25569-25578.

Hogue, C., 2001. Blowing in the wind, *Chem. Eng. News,* June 25, 2001, pp. 30-31.

Hudischewskyj, A.B. and C. Seigneur, 1989. Mathematical modeling of chemistry and physics of aerosols in plumes, *Environ. Sci. Technol.* (23): 413-421.

ICF Kaiser/SAI, 1999. Sensitivity Studies with the REMSAD Modeling System*, Draft Report SYSAPP-99/05 to U.S. Environmental Protection Agency, Office of Air Quality Planning and Standards*, Research Triangle Park, North Carolina.

IRIS, 2001. *U.S. EPA Integrated Risk Information System (IRIS)* http://www.epa.gov/iris.

Jackman, C.H, E.L. Fleming, S. Chandra, D.B. Considine, and J.E. Rosenfield, 1996. Past, present, and future modeled ozone trends with comparisons to observed trends. *J Geophys. Res*. (101): 28,753-28,767.

Jacob, D.J., J.A. Logan and P. Murti, 1999. Effects of rising Asian emissions on surface ozone in the United States, *Geophys. Res. Lett*, (26): 2175-2178.

Jacob, D.J., 2000. Heterogeneous chemistry and tropospheric ozone, 2000. *Atmos. Environ.* (34): 2131-2159.

Jacobson, M.Z., R. Lu, R.P. Turco and O.B. Toon, 1996. Development and application of a new air pollution modeling system, Part I: gas phase simulations, *Atmos. Environ.* (30): 1939-1963.

Jacobson, M.Z., 1997b. Development and application of a new air pollution modeling system – II. Aerosol module structure and design, *Atmos. Environ.* (31): 131-144.

Jacobson, M.Z., 1997c. Development and application of a new air pollution modeling system, Part III: Aerosol-phase simulations, *Atmos. Environ.* (31): 587-608.

Jacobson, M.Z., 1999. *Fundamentals of Atmospheric Modeling*, Cambridge University Press, Cambridge, United Kingdom.

Jacobson, M.Z., 2001a. GATOR-GCMM: A global- through urban-scale air pollution and weather forecast model. 1. Model design and treatment of subgrid soil, vegetation, roads, rooftops, water, sea ice, and snow, *J. Geophys. Res.* (106): 5385-5401.

Jacobson, M.Z., 2001b. Strong radiative heating due to the mixing state of black carbon in atmospheric aerosols, *Nature* (409): 695-697.

Johnston, H., 1971. Reduction of stratospheric ozone by nitrogen oxide catalysts from supersonic transport exhaust. *Science* (173):517-522.

Jones, R. L., J. Austin, D. S. McKenna, J. G. Anderson, D. W. Fahey, C. B. Farmer, L. E. Heidt, K. K. Kelly, D. M. Murphy, M. H. Proffitt, A. F. Tuck, and J. F. Vedder, 1989. Lagrangian photochemical modeling studies of the 1987 Antarctic spring vortex 1. Comparison with AAOE observations. *J. Geophys. Res.* (94):11,529-11,558.

Joos, E. and C. Seigneur, 1994. Application of a reactive plume model to a case study of pollutant oxidation and acid deposition, *Adv. Environ. Sci. Technol.* (28), Environmental Oxidants, J.O. Nriagu and M.S. Simmons, eds., pp. 137-158. John Wiley & Sons, Inc. New York, NY.

Karamchandani, P., A. Koo, C. Seigneur, 1998. A reduced gas-phase kinetic mechanism for atmospheric plume chemistry, *Environ. Sci. Technol.* (32): 1709-1720.

Karamchandani, P. and C. Seigneur, 1999. Simulation of sulfate and nitrate chemistry in power plant plumes, *J. Air Waste Manage. Assoc.* (49): PM-175-181.

Karamchandani, P., L. Santos, I. Sykes, Y. Zhang, C. Tonne, C. Seigneur, 2000. Development and evaluation of a state-of-the-science reactive plume model, *Environ. Sci. Technol.* (34): 870-880.

Karamchandani, P. C. Seigneur, Y. Zhang, 2001. Review of air quality models for acid deposition. *U.S. Environmental Protection Agency*, Washington, D.C.

Karamchandani, P., C. Seigneur, K. Vijayaraghavan and S.-Y. Wu, 2002. Development and application of a state-of-the-science plume-in-grid model, *J. Geophys. Res*. (107): 4403-4415.

Kinnison, D.E., K.E. Grant, P.S. Connell, D.A. Rotman, and D.J. Wuebbles, 1994. The chemical and radiative effects of the Mt. Pinatubo eruption. *J. Geophys. Res*. (99): 25,705-25,731.

Kley, D., P.J. Crutzen, H.G.J. Smit, H. Vömel, S.J. Oltmans, H. Grassl, and V. Ramanathan, 1996. Observations of near-zero ozone concentrations over the convective Pacific: Effects of air chemistry. *Science* (274):230-233.

Kumar, N. and A.G. Russell, 1996a. Development of a computationally efficient, reactive subgrid-scale plume model and the impact in the northeastern United States using increasing levels of chemical detail, *J. Geophys. Res.* (101): 16737-16744.

Kumar, N., M.T. Odman and A.G. Russell, 1994. Multiscale air quality modeling: application to southern California, *J. Geophys. Res.* (99): 5385-5397.

Kumar, N. and A.G. Russell, 1996b. Comparing prognostic and diagnostic meteorological fields and their impacts on photochemical air quality modeling, *Atmos. Environ.*, (30): 1989-2010.

Langmann, B. and H-F. Graf, 1997. The chemistry of the polluted atmosphere over Europe: simulations and sensitivity studies with a regional chemistry-transport model, *Atmos. Environ.* (31): 3239-3257.

Law, K.S., and J.A. Pyle, 1993. Modeling trace gas budgets in the troposphere: 1, Ozone and odd nitrogen. *J. Geophys. Res.* (98): 18,377-18,400.

Lin, C.J. and S.O. Pehkonen, 1999. The chemistry of atmospheric mercury: A review. *Atmos. Environ.* (33): 2067-2080.

Liu, X., G. Mauersberger and D. Möller, 1997. The effects of cloud processes on the tropospheric photochemistry: An improvement of the EURAD model with a coupled gaseous and aqueous chemical mechanism, *Atmos. Environ.* (31): 3119-3135.

Lu, R., R.P. Turco and M.Z. Jacobson, 1997a. An integrated air pollution modeling system for urban and regional scales: 1. Structure and performance, *J. Geophys. Res.* (102): 6063-6079.

Lu, R., R.P. Turco and M.Z. Jacobson, 1997b. An integrated air pollution modeling system for urban and regional scales: 2. Simulations for SCAQS 1987, *J. Geophys. Res.*, (102): 6081-6098.

Lurmann, F.W., D.A. Godden, and H.M. Collins. 1985. *User's guide to the PLMSTAR air quality simulation model. Environmental Research & Technology Document M-2206-100*, Newbury Park, California.

Lurmann, F.W., A.S. Wexler, S.N. Pandis, S. Musarra, N. Kumar and J.H. Seinfeld, 1997. Modeling urban and regional aerosols: II. Application to California's south coast air basin, *Atmos. Environ.* (31): 2695-2715.

Lurmann, F.W., 2000. Simplification of the UAMAERO Model for Seasonal and Annual Modeling: The UAMAERO-LT Model, *Final Report, South Coast Air Quality Management District,* Diamond Bar, California.

Mahfouf, J.F., D. Cariolle, J.-F. Royer, J.-F. Geleyn, and B. Timbal, 1993. Response of the Meteo-France climate model to changes in CO2 and sea surface temperature. *Clim. Dyn.* (9): 345-362.

Manney, G.L., L. Froidevaux, J.W. Waters, R.W. Zurek, J.C. Gille, J. B. Kumer, J. L. Mergenthaler, A. E. Roche, A. O'Neill, and R. Swinbank, 1995. Formation of low-ozone pockets in the middle stratospheric anticyclone during winter. *J. Geophys. Res.* (100):13,939-13,950.

Mathur, R., J.O. Yound, K.L. Schere and G.L. Gipson, 1998. A comparison of numerical techniques for solution of atmospheric kinetic equations, *Atmos. Environ.* (32): 1535-1553.

McElroy, M.B., R.J. Salawitch, S.C. Wofsy, and J.A. Logan, 1986. Reduction of Antarctic ozone due to synergistic interactions of chlorine and bromine. *Nature* (321):759-762.

McElroy, M.B., and R.J. Salawitch, 1989. Changing composition of the global stratosphere. *Science* (243):763-770.

McMurry, P.H. and S.K. Friedlander, 1979. New particle formation in the presence of an aerosol, *Atmos. Environ.* (13): 1635-1651.

McMurry, P.H., K.S. Woo, R. Weber, D.R. Chen and D.Y.H. Pui, 2000. Size distribution of 3 to 10 nm in atmospheric particles: implications for nucleation mechanisms, *Phil. Trans. Royal Soc. London* (A358): 2625-2642.

McRae, G.J., W.R. Goodin and J.H. Seinfeld, 1982b. Development of a second generation mathematical model for urban air pollution. I. Model formulation, *Atmos. Environ.* (16): 679-696.

McRae, G.J. and J.H. Seinfeld, 1983. Development of a second generation mathematical model for urban air pollution. II. Evaluation of model performance, *Atmos. Environ.* (17): 501-522.

Meng, Z., D. Dabdub and J.H. Seinfeld, 1998. Size-resolved and chemically resolved model of atmospheric aerosol dynamics, *J. Geophys. Res.* (103): 3419-3435.

Molina, M.J., and F.S. Rowland, 1974. Stratospheric sink for chlorofluoromethanes: Chlorine atom-catalyzed destruction of ozone. *Nature* (249):810-812.

Molina, M.J., and L.T. Molina, 1987. Production of Cl_2O_2 from the self-reaction of the ClO radical. *J. Phys. Chem.* (91):433-436.

Möller, D. and G. Mauersberger, 1995. An aqueous phase reaction mechanism. In *Clouds: Models and Mechanisms.*

Monod, A. and P. Carlier, 1999. Impact of clouds on tropospheric ozone budget: Direct effect of multiphase photochemistry of soluble organic compounds, *Atmos. Environ.* (33): 4431-4446.

Nair, H., M. Allen, L. Froidevaux, and R. W. Zurek, 1998. Localized rapid ozone loss in the northern winter stratosphere: An analysis of UARS observations. *J. Geophys. Res.* (103):1555-1571.

Nenes, A., S.N. Pandis, C. Pilinis, 1998. ISORROPIA: A new thermodynamic equilibrium model for multiphase multicomponent inorganic aerosols, *Aquatic Chem.* (4): 123-152.

Nevison, C.D., S. Solomon, and R.S. Gao, 1999. Buffering interactions in the modeled response of stratospheric O_3 to increased NO_x and HO_x. *J. Geophys. Res.* (104):3741-3754.

Odman, M.T. and A.G. Russell, 1991b. Multiscale modeling of pollutant transport and chemistry, *J. Geophys. Res.* (96): 7363-7370.

Odman, M.T., N. Kumar and A.G. Russell, 1992. A comparison of fast chemical kinetic solvers for air quality modeling, *Atmos. Environ.* (26): 1783-1789.

Odum, J.R., T. Hoffman, F. Bowman, D. Collins, R.C. Flagan and J.H. Seinfeld, 1996. Gas/particle partitioning and secondary organic aerosol yields, *Environ. Sci. Technol.* (30): 2580-2585.

Odum, J.R., T.P.W. Jungkamp, R.J. Griffin, H.J.L. Forstner, R.C. Flagan and J.H. Seinfeld, 1997. Aromatics, reformulated gasoline, and atmospheric organic aerosol formation, *Environ. Sci. Technol.*, (31): 1890-1897.

Pankow, J.F., 1994a. An absorption model of gas/particle partitioning of organic compounds in the atmosphere, *Atmos. Environ.* (28): 185-188.

Pankow, J.F., 1994b. An absorption model of gas/aerosol partitioning involved in the formation of secondary organic aerosol, *Atmos. Environ.* (28): 189-193.

Pankow, J.F., 1998. Further discussion of the octanol/air partition coefficient K_{oa} as a correlating parameter for gas/particle partitioning coefficients, *Atmos. Environ.* (32): 1493-1497.

Pirjola, L. and M. Kulmala, 2000. Aerosol dynamical model MULTIMONO, *Boreal Environ. Res.* (5): 361-374.

Pitari, G., S. Palermo, G. Visconti, and R.G. Prinn, 1992. Ozone response to a CO2 doubling: Results from a stratospheric circulation model with heterogeneous chemistry. *J. Geophys. Res*. (97): 5953-5962.

Pitari, G., V. Rizi, L. Ricciardulli, and G. Visconit, 1993. High-speed civil transport impact: The role of sulfate, nitric acid trihydrate, and ice aerosols studied with a two-dimensional model including aerosol physics. *J. Geophys. Res.* (98): 23,141-23,164.

Prather, M. J., M. B. McElroy, and S. C. Wofsy, 1984. Reductions in ozone at high concentrations of stratospheric halogens. *Nature* (312): 227-231.

Press, W.H., S.A. Teukolsky, W.T. Vetterling, B.P. Flannery, 1997. *Numerical Recipes in C, 2nd Edition.* Cambridge University Press, London, U.K.

Pun, B.K., C. Seigneur, D. Grosjean, P. Saxena, 2000. Gas-phase formation of water-soluble organic compounds in the atmosphere: a retrosynthetic analysis, *J. Atmos. Chem.* (35): 199-233.

Pun, B.K., M. Liedner, C. Seigneur, 2001. Conceptual Model for Regional Haze in the Upper Midwest. Proceedings, *Regional Haze and Global Radiation Balance – Aerosol Measurements and Models: Closure, Reconciliation and Evaluation*, Bend, OR, October 2-5, 2001.

Pun, B.K., R.J. Griffin, C. Seigneur and J.H. Seinfeld, 2002. Secondary organic aerosol: II. Thermodynamic model for gas/particle partitioning of molecular constituents, *J. Geophys. Res*., (107): 4333-4347.

Randeniya, L.K., P.F. Vohralik, I.C. Plumb and K.R. Ryan, 1997. Heterogeneous BrONO2 hydrolysis: Effect on NO2 columns and ozone at high latitudes in summer. *J. Geophys. Res*, (102): 23,543-23,557.

Richards, L.W., J.A. Anderson, D.L. Blumenthal, A. Brandt, J.A. McDonald, N. Waters, E.S. Macias, P.S. Bhardwaja, 1981. The chemistry, aerosol physics and optical properties of a western coal-fired power plant plume, *Atmos. Environ.* (15): 2111-2131.

Rind, D., D. Shindell, P. Lonergan, and N.K. Balachandran, 1998. Climate change and the middle atmosphere: Part III, The doubled CO2 climate revisited. *J. Clim.*, (11): 876-894.

Ryaboshapko, A., I.Ilyin, R. Bullock, R. Binghaus, K. Lohman, J. Munthe, G. Petersen, C. Seigneur, I. Wangberg, 2001. Intercomparison study of numerical models for long-range atmospheric transport of mercury. *Technical Report 2/2001, Cooperative Programme for Monitoring and Evaluation of the Long-range Transmission of Air Pollutants in Europe, Meteorological Synthesizing Center* – East Moscow, Russia.

Sander, S. P., R. R. Friedl, W. B. DeMore, D. M. Golden, M. J. Kurylo, R. F. Hampson, R. E. Huie, G. K. Moortgat, A. R. Ravishankara, C. E. Kolb, and M. J. Molina, 2000. *Chemical Kinetics and Photochemical Data for Use in Stratospheric Modeling, Evaluation number 13*. JPL Publication 00-3, Pasadena, California.

Saxena, P. and L.M. Hildemann, 1996. Water-soluble organics in atmospheric particles: a critical review of the literature and application of thermodynamics to identify candidate compounds, *J. Atmos. Chem.* (24): 57-109.

Scire, J.S., D.G. Strimaitis, R.J. Yamartino, 1990. *Model formulation and user's guide for the CALPUFF dispersion model*, Earth Tech Concord MA.

Schroeder, W.H. and J. Munthe, 1998. Atmospheric mercury: An overview, *Atmos. Environ.* (32): 809-822.

Schmidt, H., C. Derognat, R. Vautard and M. Beekmann, 2001. A comparison of simulated and observed ozone mixing ratios for the summer of 19998 in Western Europe, *Atmos. Environ*. (35): 6277-6297.

Seigneur, C., 1982. A model of sulfate aerosol dynamics in atmospheric plumes, *Atmos. Environ.* (16): 2207-2228.

Seigneur, C., T.W. Tesche, P.M. Roth, M.-K. Liu. 1983. On the treatment of point source emissions in urban air quality modeling. *Atmos. Environ.*, (17):1655-1676.

Seigneur, C. and H.M. Barnes, 1986. Technical considerations in regional aerosol modeling, *in Air Pollution Modeling and Its Applications, Vol. 5*, C. De Wispelaere, F.A. Schiermeier and N.V. Gillani, eds., pp. 343-369, Plenum Press, New York.

Seigneur, C. 1987. Computer simulation of air pollution chemistry. *Environ. Software,* (2):116.

Seigneur, C. and E. Constantinou, 1995 Chemical kinetic mechanism for atmospheric chromium, *Environ. Sci. Technol.* (29): 223-231.

Seigneur, C., X.A. Wu, E. Constantinou, P. Gillespie, R.W. Bergstrom, I. Sykes, A. Venkatram, P. Karamchandani, 1997. Formulation of a second-generation reactive plume and visibility model, *J. Air Waste Manage. Assoc.* (47): 176-184.

Seigneur, C., H. Abeck, G. Chia, M. Reinhard, N. Bloom, E. Prestbo, and P. Saxena, 1998. Mercury adsorption to elemental carbon (soot) particles and atmospheric particulate matter, *Atmos. Environ.* (32): 2649-2657.

Seigneur, C., P. Pai, I. Tombach, C. McDade, P. Saxena, P. Mueller. 2000. Modeling of potential power plant plume impacts on Dallas Fort Worth visibility, *J. Air Waste Manage. Assoc.* (50): 835-848.

Seigneur, C. and P. Karamchandani, 2001. Review of the State of the Science for Modeling Atmospheric Particulate Matter*, report for Renault*, Guyancourt, France.

Seinfeld J.H. and S.N. Pandis, 1998. *Atmospheric chemistry and Physics.* John Wiley and Sons, New York, NY.

Sheridan, P.J., C.A. Brock, and J.C. Wilson, 1994. Aerosol particles in the upper troposphere and lower stratosphere: Elemental composition and morphology of individual particles in northern midlatitudes. *Geophys. Res. Lett.* (21): 2587-2590.

Shindell, D.T., 2001. Climate and ozone response to increased stratospheric water vapor. *Geophys. Res. Lett.* (28): 1551-1554.

Smyshlyaev, S.P., and V.A. Yudin, 1995. Numerical simulation of the aviation release impact on the ozone layer. *Izv. Atmos. Oceanic Phys*. (31): 116-125.

Solomon, S., R.R. Garcia, F.S. Rowland, and D.J. Wuebbles, 1986. On the depletion of Antarctic ozone. *Nature* (321): 755-758.

Solomon, S., R.W. Sanders, and H.L. Miller, Jr., 1990. Visible and near-ultraviolet spectroscopy at McMurdo Station, Antarctica 7. OClO diurnal photochemistry and implications for ozone destruction. *J. Geophys. Res.*, (95):13,807-13,817.

Solomon, S., R.R. Garcia, and A.R. Ravishankara, 1994. On the role of iodine in ozone depletion. *J. Geophys. Res.*, (99):20,491-20,499.

Solomon, S., 1999. Stratospheric ozone depletion: A review of concepts and history. *Rev. Geophys.*, (37): 275-316.

Song, C.H. and G.R. Carmichael, 1999. A modeling investigation on tropospheric aerosols over East Asia: I. Model description, *J. Geophys. Res.*, submitted.

Spicer, C.W., E.G. Chapman, B.J. Finlayson-Pitts, R.A. Plastridge, J.M. Hubbe, J.D. Fast, C.M. Berkowitz, 1998. Unexpectedly high concentrations of molecular chlorine in coastal air, *Nature* (394): 353-3656.

Staehelin, J.,N. R.P. Harris, C. Appenzeller, and J. Eberhard, 2001. Ozone trends: A review. *Rev. Geophys.* (39):231-290.

Steil, B., M. Demeris, C. Bruhl, P.J. Crutzen, V. Grewe, M. Ponater, and R. Sauser, 1998. Development of a chemistry module for GCMs: First results of a multi-annual integration. *Ann. Geophys*. (16): 205-228.

Stewart, D.A., M.K. Liu, 1981. Development and application of a reactive plume model. *Atmos. Environ.*. (15): 2377-2393.

Stolarski, R.S., and R.J. Cicerone, 1974. Stratospheric chlorine: A possible sink for ozone. *Can. J. Chem.* (52): 1610-1615.

Sykes, R.I., S.F. Parker, D.S. Henn, W.S. Lewellen, 1993. Numerical simulation of ANATEX tracer data using a turbulence closure model for long-range dispersion, *J. Appli. Met.* (32): 929-947.

Sykes, R.I. and D.S. Henn, 1995. Representation of velocity gradient effects in a Gaussian puff model, *J. Appli. Met.* (34): 2715-2737.

Tesche, T.W., C. Seigneur, W.R. Oliver, and J.L. Haney 1984. Modeling ozone control strategies in Los Angeles. *J. Environ. Eng.*, (110): 208-225.

Toon, O.B., P. Hamill, R.P. Turco, and J. Pinto, 1986. Condensation of HNO_3 and HCl in the winter polar stratosphere. *Geophys. Res. Lett.* (13):1284-1287.

Wamsley, P.R., et al., 1998. Distribution of halon-1211 in the upper troposphere and lower stratosphere and the 1994 total bromine budget. *J. Geophys. Res.* (103):1513-1526.

Warneck, P., 1988. *Chemistry of the natural atmosphere*, Academic Press, San Diego, CA.
Wayland, R.J., 1999. REMSAD – 1990 Base Case Simulation: Model Performance Evaluation – Annual Average Statistics, *U.S. Environmental Protection Agency, Office of Air Quality Planning and Standards* (OAQPS), Research Triangle Park, North Carolina.

Wayne, R.P., 1991. *Chemistry of the atmospheres, 2nd edition*, Clarendon Press, Oxford, U.K.

Webster, C.R., H.A. Michelsen, M.R. Gunson, J.J. Margitan, J.M. Russell III, G.C. Toon, and W.A. Traub, 2000. Response of lower stratospheric HCl/Cly to volcanic aerosol: Observations from aircraft, balloon, space shuttle, and satellite instruments. *J. Geophys. Res.* (105): 11,711-11,719.

Weisenstein, D.K., M.K.W. Ko, E.G. Dyominov, G. Pitari, L. Ricciardulli, G. Visconti, and S. Bekki, 1998. The effects of sulfur emissions from HSCT aircraft: A 2-D model intercomparison. *J. Geophys. Res.*, (103): 1527-1547.

Wexler, A.S., F.W. Lurmann and J.H. Seinfeld, 1994. Modeling urban and regional aerosols, I. Model development, *Atmos. Environ.* (28): 531-546.

Wilkening, K.E., L.A. Barrie, and M. Engle, 2000. Trans-Pacific air pollution. *Science* (290): 65-67.

Wofsy, S.C., M.B. McElroy, and Y.L. Yung, 1975. The chemistry of atmospheric bromine. *Geophys. Res. Lett.* (2): 215-218.

Woo, K.S., D.R. Chen, D.Y.H. Pui and P.H. McMurry, 2001. Measurement of Atlanta aerosol size distributions: observations of ultrafine particle events, *Aerosol Sci. Technol.* (34): 75-87.

World Meteorological Organization/United Nations Environmental Programme (WMO/UNEP). 1999. *Scientific assessment of ozone depletion: 1998*., Global Ozone Research and Monitoring Project, Report 44, Geneva, Chapters 1, 4, 5, 11, 12.

Yu, J. R.J. Griffin, D.R. Cocker III, R.C. Flagan, J.H Seinfeld, 1999. Observation of gaseous and particulate products of monoterpene oxidation in forest atmospheres. *Geophys. Res. Lett.* (26): 1145-1148.

Zannetti, P. 1990. *Air Pollution Modeling*. Van Nostrand Reinhold, New York, NY.

Zerefos, C.S., K. Tourpali, B.R. Bojkov, D.S. Balis, B. Rognerud, and I.S.A. Isaksen, 1997. Solar activity-total column ozone relationships, observations and model studies with heterogeneous chemistry, *J. Geophys. Res.* (102):1561-1569.

Zhang, R., P.J. Wooldridge, J.P. D. Abbatt, and M.J. Molina, 1993. Physical chemistry of the H_2SO_4/H_2O binary system at low temperatures: Stratospheric implications. *J. Phys. Chem.* (91): 433-436.

Zhang, Y., 1994. *The chemical role of mineral aerosols in the troposphere in east Asia*, Ph.D. thesis, Department of Chemical and Biochemical Engineering, University of Iowa, Iowa City, Iowa.

Zhang, Y., C. Seigneur, J.H. Seinfeld, M.Z. Jacobson and F. Binkowski, 1999. A comparative review of algorithms used in air quality models, *Aerosol Sci. Technol.* (31): 487-514.

Zhang, Y., C. Seigneur, J.H. Seinfeld, M. Jacobson, S.L. Clegg and F.S. Binkowski, 2000. A comparative review of inorganic aerosol thermodynamic equilibrium modules: Similarities, differences, and their likely causes, *Atmos. Environ.* (34): 117-137.

Zhang, Y., B. Pun, K. Vijayaraghavan, S.-Y. Wu, C. Seigneur, S. Pandis, M. Jacobson, A. Nenes and J.H. Seinfeld, 2004, Development and application of the Model of Aerosol Dynamics, Reaction, Ionization and Dissolution, *J. Geophys. Res*. (109): D01202, doi:10.1029/2003JD003501.